AD-A183 517 BLUE-GREEN LASER DIODE RESEARCH PROGRAM(U) MINNESOTA MINING AND MFG CO ST PAUL ELECTRONIC AND INFORMATION SECTOR LAB J E POTTS ET AL. JUL 87 N00014-85-C-0552 1/1

UNCLASSIFIED F/G 9/3 NL

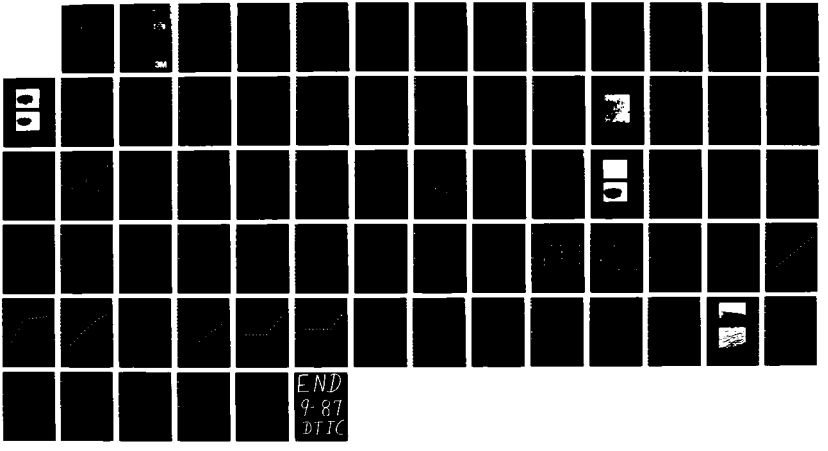

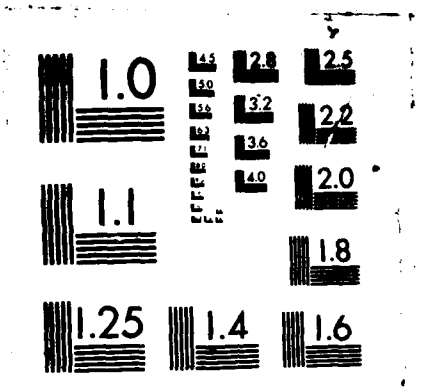

(12)

DTIC FILE COPY

BLUE-GREEN LASER DIODE RESEARCH PROGRAM

Quarterly Technical Progress Report No. 5
For The Period April 1, 1987 To June 30, 1987

Prepared Under
Contract Number N00014-85-C-0552

JULY, 1987

APPPROVED FOR PUBLIC RELEASE
DISTRIBUTION UNLIMITED

The views and conclusions contained in this document are those of the authors and should not be interpreted as necessarily representing the official policies, either expressed or implied, of the Defense Advanced Research Projects Agency or the U.S. Government.

Work supported in part by the:

DEFENSE ADVANCED RESEARCH PROJECTS AGENCY
1400 Wilson Boulevard
Arlington, VA 22209

Under the:

OFFICE OF NAVAL RESEARCH
Department Of The Navy
800 N. Quincy Street
Arlington, VA 22217-5000

Electronic and Information
Sector Laboratories/3M

St. Paul, MN 55144-1000

3M

UNCLASSIFIED

SECURITY CLASSIFICATION OF THIS PAGE

AD A183517

REPORT DOCUMENTATION PAGE

1a. REPORT SECURITY CLASSIFICATION UNCLASSIFIED	1b. RESTRICTIVE MARKINGS
2a. SECURITY CLASSIFICATION AUTHORITY	3. DISTRIBUTION/AVAILABILITY OF REPORT Approved for Public Release Distribution Unlimited
2b. DECLASSIFICATION/DOWNGRADING SCHEDULE	
4. PERFORMING ORGANIZATION REPORT NUMBER(S) Quarterly Technical Progress Report No. 5	5. MONITORING ORGANIZATION REPORT NUMBER(S)
6a. NAME OF PERFORMING ORGANIZATION 3M Company 6b. OFFICE SYMBOL (If applicable)	7a. NAME OF MONITORING ORGANIZATION Defense Advanced Research Projects Agency
6c. ADDRESS (City, State and ZIP Code) E&I Sector Laboratory - 201-IN-36 3M Center - St. Paul, MN 55144	7b. ADDRESS (City, State and ZIP Code) 1400 Wilson Boulevard Arlington, VA 22209
8a. NAME OF FUNDING/SPONSORING ORGANIZATION Office of Naval Research 8b. OFFICE SYMBOL (If applicable)	9. PROCUREMENT INSTRUMENT IDENTIFICATION NUMBER Contract No. N00014-85-C-0552
8c. ADDRESS (City, State and ZIP Code) Dept. of the Navy 800 N. Quincy St. Arlington, VA 22217-5000	10 SOURCE OF FUNDING NOS PROGRAM ELEMENT NO / PROJECT NO / TASK NO / WORK UNIT NO
11 TITLE (Include Security Classification) Blue-Green Laser Diode Research Program	
12. PERSONAL AUTHOR(S) Drs. J. E. Potts, H. A. Mar, and C. T. Walker	
13a. TYPE OF REPORT Technical Progress 13b. TIME COVERED FROM 87/04/01 TO 87/06/30	14 DATE OF REPORT (Yr. Mo. Day) 1987, July 15 PAGE COUNT 71
16 SUPPLEMENTARY NOTATION	
17 COSATI CODES FIELD / GROUP / SUB GR	18 SUBJECT TERMS (Continue on reverse if necessary and identify by block number) Blue-Green Laser or Lasers, Blue-Green

19 ABSTRACT (Continue on reverse if necessary and identify by block number)

The ZnSe materials work (Task I) was devoted almost exclusively to various attempts at p-doping, and some of the results are quite encouraging. The laboratories have tried both Na- and Li-doping, and have completed work on Sb-doping, including some laser-assisted incorporation of Sb. Using a "clean" source of Na, the laboratories were able to incorporate larger concentrations of Na without a significant increase in unintentionally-incorporated extrinsic donors, as was the case when the Na$_2$Se compound source was used. Na appears to be well-behaved in the sense that the incorporated-Na concentration increases in proportion to the incident Na flux. However, the films remain n-type, albeit of high resistivity, even at the highest Na concentrations. In addition, the photoluminescence (PL) in high-Na concentration films [illegible] implying the presence of structural defects, perhaps due to the [illegible] intrinsic properties of Na as an acceptor [illegible] were thwarted by the simultaneous incorporation [illegible]

20 [illegible]

UNCLASSIFIED/UNLIMITED [illegible]

22a NAME OF RESPONSIBLE INDIVIDUAL

DD FORM 1473, 83 APR

EXECUTIVE SUMMARY

The ZnSe materials work (Task 1) during the past quarter has been devoted almost exclusively to various attempts at p-doping, and some of the results are quite encouraging. The St. Paul group has tried both Na- and Li-doping, while the Toronto group has completed its work on Sb-doping, including some laser-assisted incorporation of Sb.

Using a "clean" source of Na, we have been able to incorporate larger concentrations of Na without a concomitant increase in unintentionally-incorporated extrinsic donors, as was the case when we used the Na_2Se compound source. Na appears to be well-behaved in the sense that the incorporated-Na concentration increases in direct proportion to the incident Na flux. However, the films remain n-type, albeit of high resistivity, even at the highest Na concentrations. In addition, the photoluminescence (PL) in high-Na-concentration films show large broad emission near 2.60 eV, implying the presence of structural defects, perhaps induced by the Na atoms themselves. With this study we are, for the first time, exploring the intrinsic properties of Na as an acceptor dopant in ZnSe; previous attempts have been flawed by the simultaneous incorporation of unintentionally-incorporated donors.

Li has previously been reported to have been used for successful n-to-p conversion of ZnSe grown by a vapor phase transport process and by organometallic chemical vapor deposition, although both of those reports have been met with some skepticism. Our Li-doping has, at these early stages, shown greater promise than has the Na-doping work.

We have been able to incorporate Li up to $3 \times 10^{18} cm^{-3}$. PL spectra have shown dominant acceptor-bound-exciton emission with almost no donor-bound-exciton or donor-acceptor-pair emission. Electrical measurements, while not quantitative because of the high resistivities of the films, give clear indications that the material is p-type. This constitutes the first demonstration of p-ZnSe by MBE! A variety of impurities appear in the SIMS analysis of the films. Work is underway to find a "cleaner" Li source.

The Sb-doping work begun during the previous quarter was extended by examining the dependence of Sb incorporation on various growth parameters

A-1

(T_G, T_{Sb} and BPR = P_{Zn}/P_{Se}). Sb incorporation coefficients varied from 10^{-2} to 1 as T_G is decreased from 330 to 250°C, and the Sb concentration could be increased from 5 x 10^{15} up to 5 x 10^{19} cm^{-3} at T_G = 330°C by increasing the Sb cell temperature, T_{Sb}. Contrary to expectations, the Sb incorporation was not enhanced by using a large BPR. In spite of the large Sb incorporation, photoluminescence measurements indicate that Sb does not form simple Sb_{Se}; in particular, no evidence for acceptor-bound-exciton emission attributable to Sb is seen.

Laser-assisted MBE growth of Sb-doped ZnSe showed improved film quality, as judged by RHEED and photoluminescence, but there still appeared to be no evidence of incorporation of Sb as a shallow hydrogenic acceptor. Sb would appear to be an unsuitable p-dopant for ZnSe.

Also during this past quarter, we have extended our study of the tilt between ZnSe epilayer and Ge substrate by studying the tilt as a function of the cut-off angle of the substrate and of the total film thickness. Electron-beam pumping measurements on cavities formed from MBE and OMVPE films have shown consistently lower lasing thresholds for the MBE-grown films; the differences have been traced to the poorer surface morphology for the OMVPE films. Finally, our earlier theoretical treatment of the two-dimensional electron gas (2DEG) in ZnSe at a lattice-matched ZnSe-$ZnS_{1-X}Te_X$ (X = 0.37) heterojunction has been extended to modeling the electron transport in the 2DEG at the interface. The maximum channel conductivity has been calculated as a function of spacer width and the electron concentrations needed for maximization at each spacer width are reported.

TABLE OF CONTENTS

LIST OF FIGURES

LIST OF FIGURES (continued)

LIST OF FIGURES (continued)

LIST OF TABLES

1.0 INTRODUCTION

This report covers progress during the nineteenth through twenty-first months of ONR Contract N00014-85-C-0552. The various sections of the report are numbered and titled using the format of the original proposal. As before, results from parallel programs at 3M-St. Paul and 3M-Toronto are discussed.

2.0 PROGRESS REPORT

2.1 Project 1, Task 1: Materials Research - Undoped ZnSe Research

During the past quarter, there was less emphasis placed on the growth and analysis of unintentionally-doped ZnSe in order to devote more effort to the p-doping work (Project 1, Task 2). There have, however, been some developments regarding variations in the purity of the Se starting materials. In addition, the (2 x 1) surface reconstruction from ZnSe layers observed in the 3M Canada growth system has been investigated further. Finally, additional studies of the tilt between (100) Ge and the ZnSe epilayer using double-crystal X-ray rocking curve measurements and electron microscopy have been performed.

2.1.1 Unintentionally-Doped ZnSe Heteroepitaxy on (100) GaAs

2.1.1.1 Growth of Unintentionally-Doped ZnSe on (100) GaAs

As we discussed in Quarterly Progress Report No. 3, the Se starting material plays a most important role in achieving uncompensated high-resistivity ZnSe films. We believe that the low concentration of Group VII elements, particularly Cl, in the 6N+ super-grade Se supplied by Osaka Asaki Metals is responsible for the dramatic improvement which we have seen. However, after several Se charges from the same lot had been used, possible variations in the quality of this Se were observed. The undoped ZnSe film grown as a check run after the latest source reloading shows a dominant donor-bound exciton emission in the low-temperature photoluminescence, and has an n-type electrical conductivity with an electron carrier concentration of $9 \times 10^{15} cm^{-3}$. These results are similar to those which we obtained earlier using Se source material from other vendors. We tentatively attribute this variation to variations in the Group VII content of the starting charge. In most purity analyses, nonmetallic impurities are not taken into account and most suppliers do not pay much attention to them. We find it significant that, as more material from the starting charge is consumed, the quality of the undoped film is improved and, eventually, the characteristics of a high-quality undoped film, namely dominant free-exciton

emission in PL and very low residual carrier concentration, are restored. But the time involved in this in-situ purification is substantial. It seems that a screening procedure for testing the Se charges prior to loading into the MBE system is of vital importance. We are currently considering various possible screening procedures.

2.1.1.2 Investigation of Surface Reconstruction from Undoped ZnSe

It was noted in an earlier report that, since moving to the 6N+ super-grade Se source material, (2 x 1) surface reconstruction was observed from ZnSe layers grown at the 3M Toronto Lab. This phenomenon has been further investigated in this trimester period.

The principal finding is that the 1/2-order diffraction lines in the [0$\bar{1}$1] azimuth are indicative of a Se-stabilized surface. The intensity of the 1/2-order lines and therefore the degree of Se-stabilization can be controlled by the Se flux for a fixed Zn flux. Examples of two Se-stabilized surfaces are shown in Figures 2-1 (a) and (b). Figure 2-1(a) illustrates the RHEED pattern recorded from a layer grown using a 1:2 Zn/Se ratio while Figure 2-1(b) shows the pattern observed from a layer grown using a 1:4 beam pressure ratio. Note that the surface shown in Figure 2-1(a) is only very weakly Se-stabilized while that shown in Figure 2-1(b) is quite strongly Se-stabilized. In both cases the substrate temperature was 330°C. It is also worth noting that the 1/2-order diffraction lines were observed in the primary [0$\bar{1}$1] azimuth. This result, therefore, is in agreement with observations reported earlier by the St. Paul Lab.

2.1.2 X-Ray Study of Tilt of ZnSe/(100)Ge Epilayers

2.1.2.1 Double Crystal Rocking Curve (DCRC) Analysis

As a result of our previous studies it was found that tilting of the epilayer planes with respect to the same planes in the substrate is a complex phenomena. In order to shed more light onto this problem, the behavior of the tilt angle as a function of the cut-off angle of the substrate and as a function of total film thickness was studied.

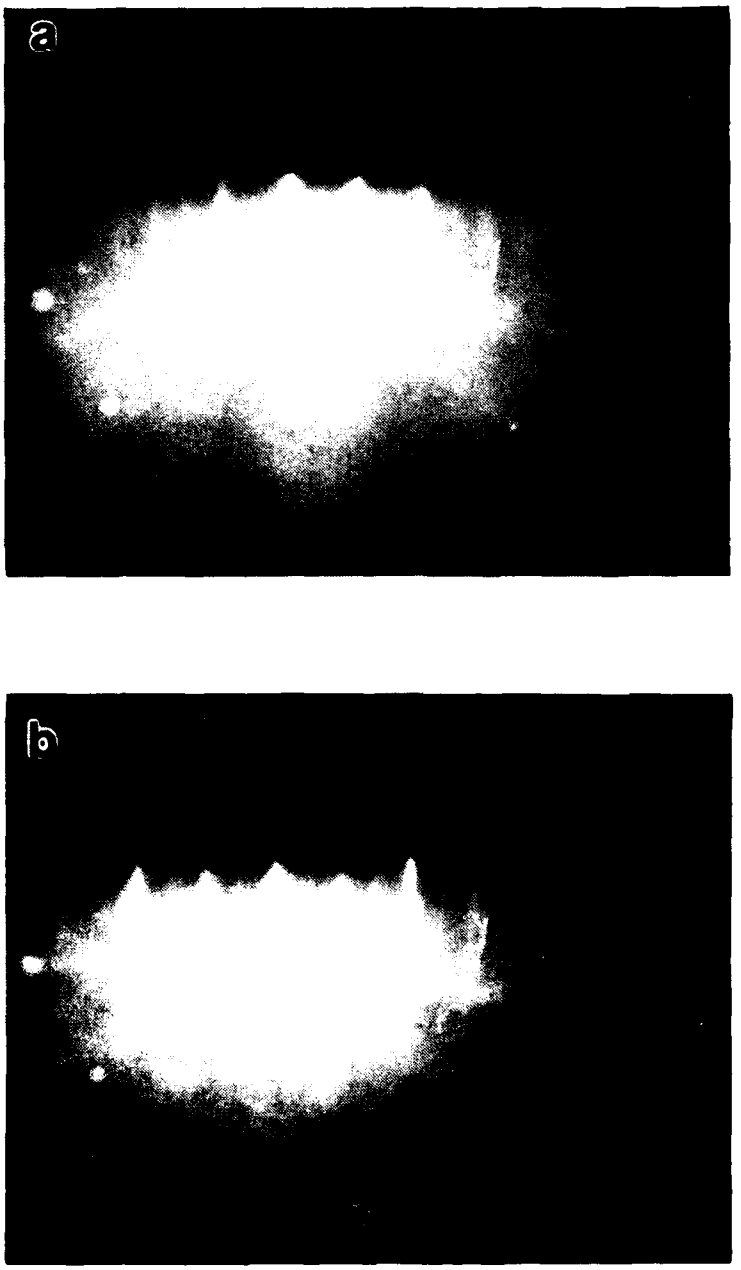

Figure 2-1. RHEED patterns recorded in the [011] azimuth for two Se-stabilized surfaces at T_s = 330°C and using Zn/Se ratios of (a) 1:2 and (b) 1:4. 1/2-order diffraction lines indicative of Se-stabilized surfaces can be seen in the patterns.

Figure 2-2 shows the tilt angle between (004) planes of ZnSe and Ge as a function of the cut-off angle of the Ge surface. In all cases the surface of Ge was cut-off towards the [110] direction. Film thickness in all experiments was kept around 1.2 - 1.5 μm. As can be seen from Figure 2-2, the tilting of the layers is monotonically decreasing with decreasing cut-off angle. There is no indication that there is a critical cut-off angle for the investigated series of samples where the epitaxy is parallel (i.e., $\Delta\phi = 0$) as suggested by Nagai [1]. Our previous measurements of the tile angle, performed on a similar series of samples grown to 4 - 4.5 μm indicated however that there is a critical cut-off angle where the value of the tilt angle goes through a minimum. These result indicate that parallel epitaxy conditions depend on a number of parameters and not related simply to the cut-off angle. Work is now in progress to check this point.

Figure 2-3 represents result obtained from measurements of tilt on a number of samples grown to various thicknesses. The cut-off angle was kept constant at $\simeq 2^\circ$ for this series. The very interesting result as can be seen from Figure 2-3 is that tilt angle dependence on thickness can be described by two distinctly different slopes. These results are presently under examination and we are trying to build a model which will explain the findings present in Figure 2-3.

It should be noted here that the measurement of the tilt angle is correct only if a full rotation of the sample around the surface normal is performed.

A model has been developed recently in our laboratory in which it was shown [2] that in order to obtain the true value of the tilt between substrate and epilayer planes by DCRC analysis, it is necessary to perform a complete 0° to 360° rotation of the sample about its normal as opposed to randomly selecting a pair of measurements separated by 180°, a technique which is commonly adopted today [1].

It is well known that a DCRC signal from a thin epilayer grown on a single crystal substrate consists of two peaks, one from the epilayer and one from the substrate, if the conditions defined by DuMond [3] are fulfilled.

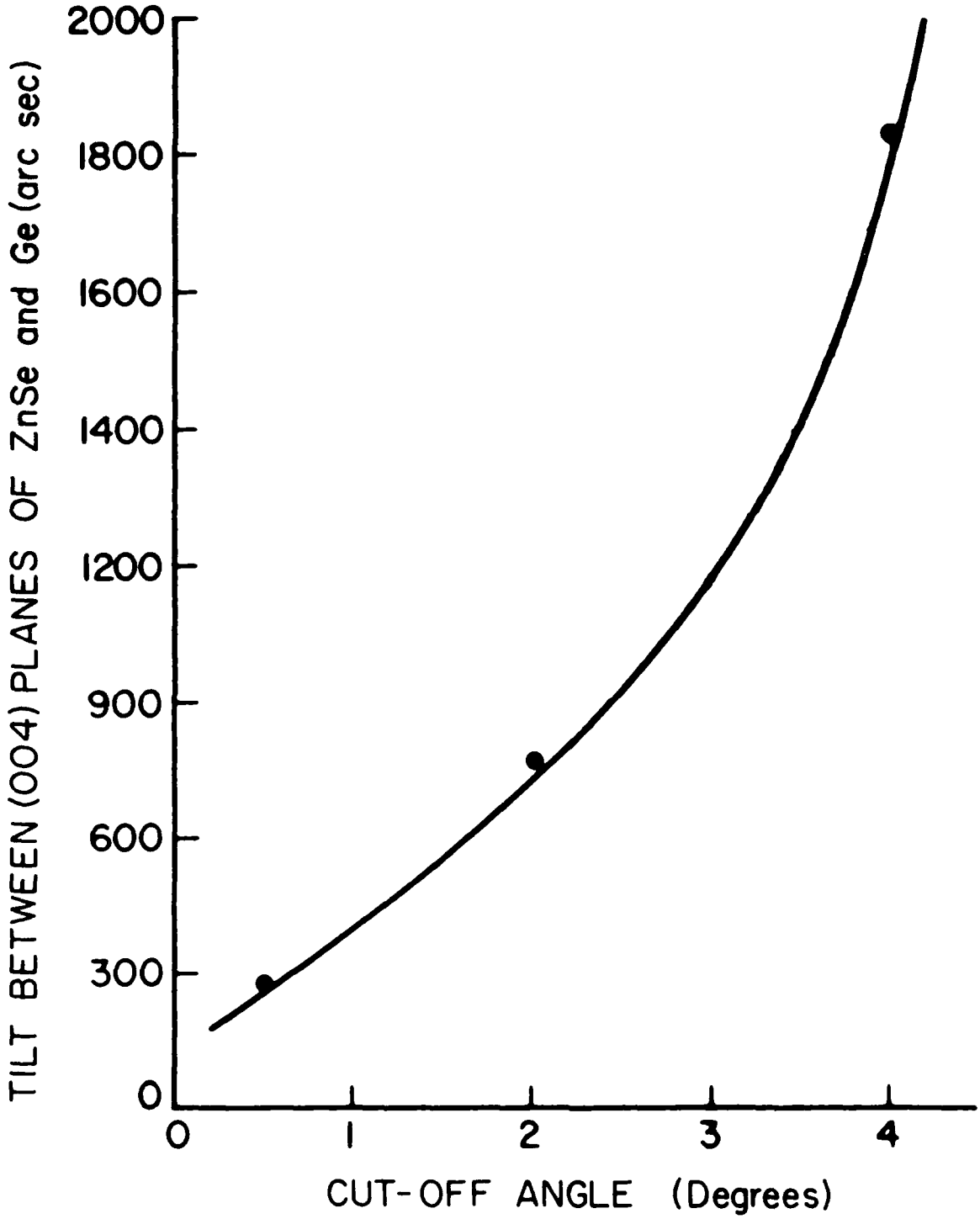

Figure 2-2. Tilt angle as a function of the cut-off angle of the Ge substrate surface.

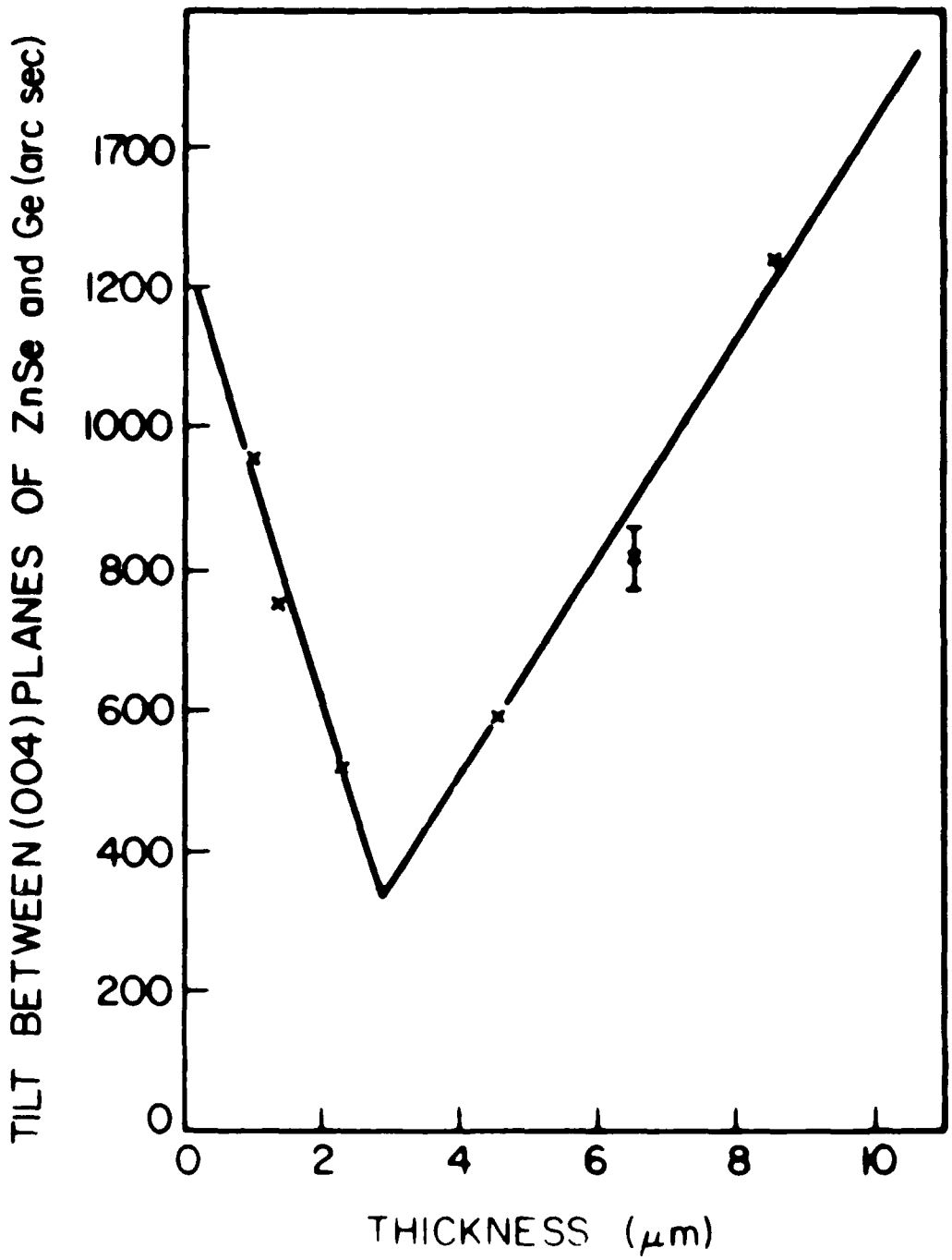
TILT BETWEEN (004) PLANES OF ZnSe and Ge (arc sec)
1700
1200
1000
800
600
400
200
0
0
2
4
6
8
10
THICKNESS (μm)

Figure 2.3.

For epilayer planes tilted in a particular crystallographic orientation with respect to the substrate planes the difference in angle between the Bragg peaks, (ΔD), is due to two effects; mismatch between the film and the substrate lattice $\Delta\theta$, and misorientation (tilt) between the similar planes in both crystals, ($\Delta\phi$) (Figure 2-4(b)). These effects are readily separated by using the following expressions [4]:

$$\Delta\theta = 1/2\ (\Delta D_{max} + \Delta D_{min}) \qquad .....(1)$$

$$\Delta\phi = 1/2\ (\Delta D_{max} - \Delta D_{min}) \qquad .....(2)$$

where ΔD_{max} and ΔD_{min} are the maximum and minimum separation between the epilayer and the substrate peaks, respectively. The full separation, ΔD, between the peaks at any given angular position of the sample can be expressed by

$$\Delta D = \Delta\theta + \Delta\phi \cos\alpha \qquad .....(3)$$

where α is a rotation angle of the incident beam around the normal to the reflection plane, or in the case of a fixed beam, a rotation angle of the sample around the normal to the reflection plane. Equation No. 3 can be expressed graphically, as shown in Figure 2-4(a), which represents two general cases of samples with the same mismatch, $\Delta\theta$, but with various degrees of tilting between the epilayer and the substrate planes. Depending on the relative values of $\Delta\theta$ and $\Delta\phi$ the cosinusoidal curve will lie above the abscissa, or will intersect it. For $\Delta\theta > \Delta\phi$ the former situation will apply as shown by curve 1 in Figure 2-4(a), while for $\Delta\theta < \Delta\phi$ the situation represented by curve 2 in Figure 2-4(a) will apply.

It is clear, therefore, that taking any two 180° separated measurements (ΔD_1 and ΔD_2) which is commonly adopted technique [1, 5, 6] and calculating $\Delta\phi$ using Equation No. 2 will result in an erroneous value for the tilt. A characteristic example is the points A and B on Figure 2-4(a). If these two values of peak separation would be taken as ΔD_1 and ΔD_2, then for both cases shown in Figure 2-4(a) the conclusion would be that $\Delta\phi = 0$; i.e., no tilt present in the grown epilayers. As it is clear from Figure 2-4(a), only from the pair of measurements performed at 0° (A) and 180° position the true values of the mismatch and the tilt would be obtained.

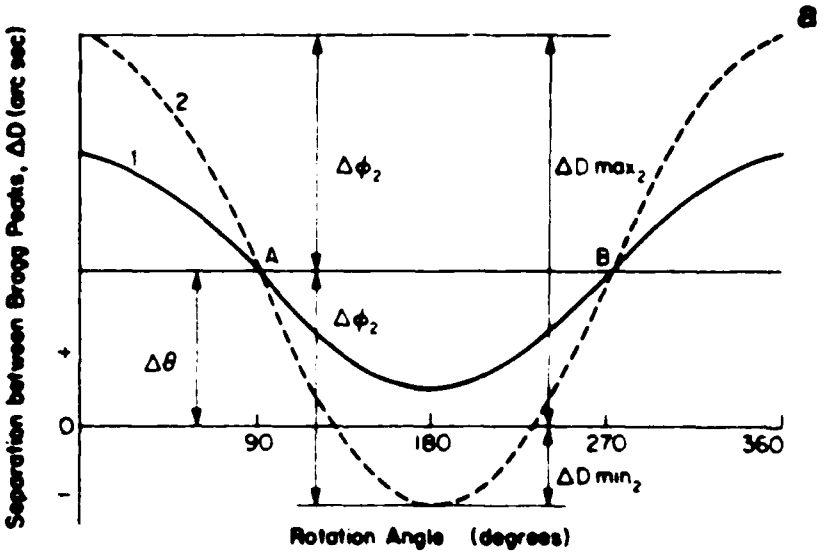

Figure 2-4(a). Graphical representation of equation 3 (see text), i.e., the dependence of the separation between epilayer and substrate Bragg peaks on angular position of the sample. Note: All values with subscript 2 refer to curve 2. The same values for curve 1 are not shown.

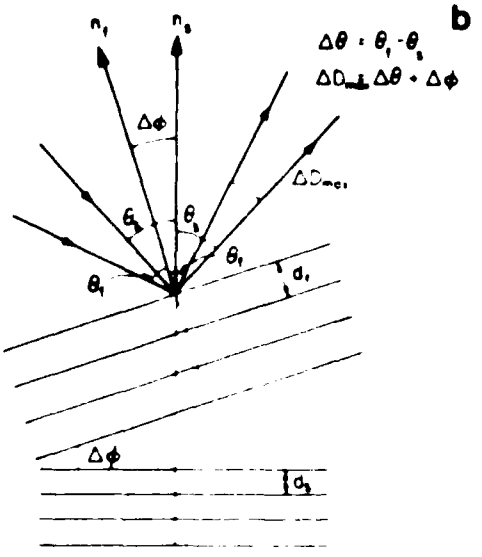

Figure 2-4(b). Principle of the measurement of the angle between the planes of the film (f) and the substrate (s). θ_f and θ_s are the Bragg angles for the epilayer and the substrate, respectively, n_f and n_s are the normals to the diffracting planes of the epilayer and the substrate.

It should be noted that once a full rotation of the sample is performed and a graph similar to Figure 2-4(a) is plotted, the values of $\Delta\theta$ and $\Delta\phi$ could be extracted graphically [4] as shown in Figure 2-4(a). Using this procedure, the strain, tilt, and lattice constants could be readily obtained.

It is obvious, therefore, that a randomly chosen pair of DCRC measurements separated by 180° may lead to erroneous values of layer tilt.

In order to demonstrate the phenomena described above, we performed DCRC analysis on a number of samples with various degrees of tilt between the (001) planes of the epilayer and the substrate.

Figure 2-5 shows the separation between (004) Bragg peaks as a function of the angular position of the sample as measured for ZnSe/(100) GaAs [Figures 2-5(a) and (b)] and ZnSe/(100) Ge [Figure 2-5(c)]. Also shown in Figure 2-5 for all three cases are the calculated separation between the (004) peaks, ΔD, as a function of angular position of the sample by using Equation No. 3. For this calculation the $\Delta\theta$ and $\Delta\phi$ values as derived from the experimental curves of Figure 2-5 were used. As can be seen from comparison of the experimental and calculated curves of $\Delta D(\alpha)$ the measured values of ΔD do not follow a simple cosinusoidal relationship.

The deviation of ΔD from an ideal cosinusoidal behavior could be due to a number of factors. It is possible that during the rotation of the sample around the surface normal slightly different areas of the sample were exposed to the X-ray beam at each angular position. If the tilt or the mismatch are not homogeneous through the layer, then the ΔD values measured at each position will deviate from a simple cosinusoidal variation with the rotation angle. Another possible reason is the presence of a complex tilt along more than one well defined crystallographic orientation.

A few samples doped with Sb to various levels were also checked with DCRC. As can be seen from Figure 2-6 the lattice constant of ZnSe was found to be dependent on the doping level; i.e., increasing as the doping level increases.

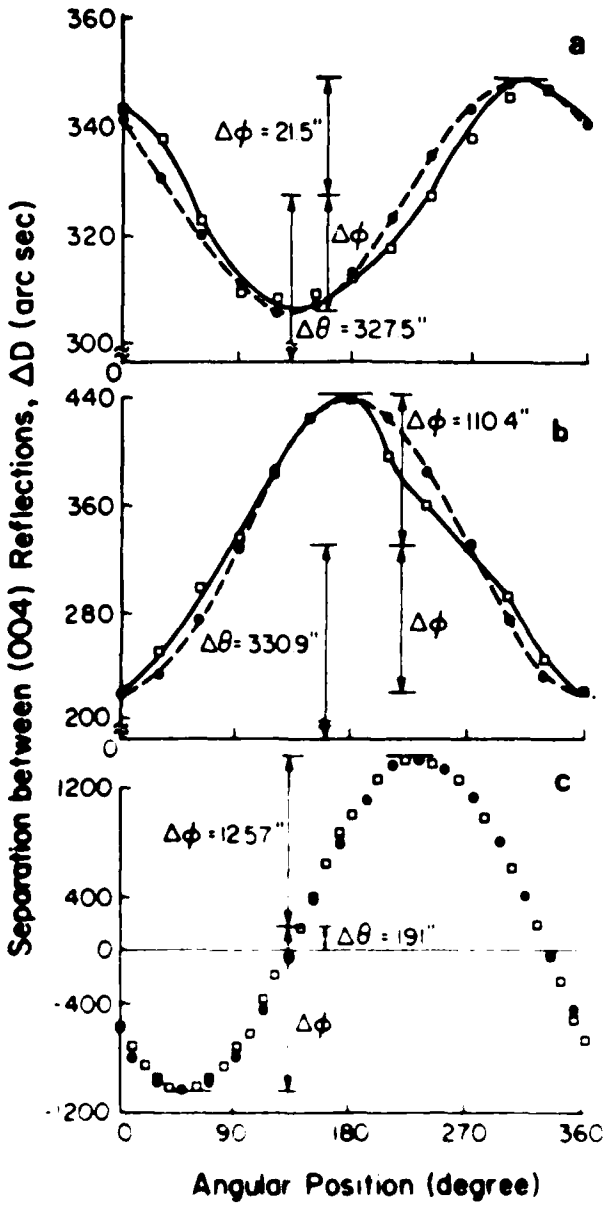

Figure 2-5. Examples of separation between (004) peaks diffracted from the substrate and the epilayer as a function of angular position of the sample as measured for (a), (b) ZnSe film grown on (100) GaAs substrate, (c) ZnSe film grown on (100) Ge substrate (open squares), and as calculated using Δθ and Δφ values from the measured data (full dots).

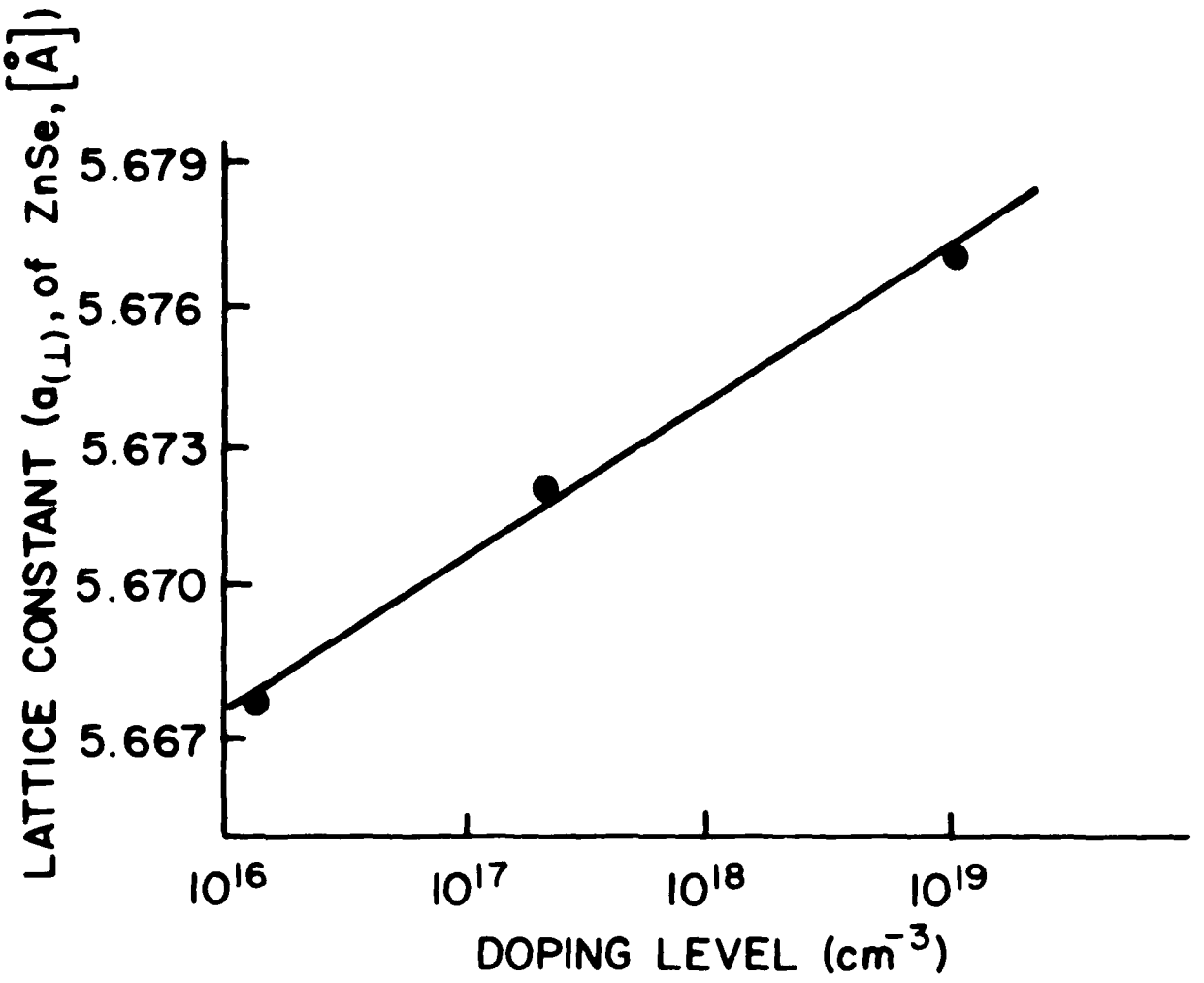

Figure 2-6. Lattice constant of ZnSe (measured normal to the interface) as a function of Sb doping level.

The fact that the lattice parameter is sensitive to doping levels as low as $10^{16}(cm^{-3})$ can be used in routine work to estimate the doping levels when an initial calibration is performed with SIMS.

2.1.2.2 Conventional Transmission Electron Microscopy

Additional confirmation of the finding that ZnSe/(100) Ge system is growing with a cellular structure [7] was obtained from a few samples of ZnSe grown on (100) Ge. Figure 2-7 demonstrates a ZnSe thin layer as viewed in planar mode; i.e., with the (001) axis parallel to the e-beam direction. The cell structure of the film is clearly visible. Also, an intricate net of dislocations can be seen in the picture.

2.2 Project 1, Task 2: Materials Research - p-ZnSe

Considerable progress has been made in the studies of a variety of potential p-type dopants in ZnSe during the past quarter. Li shows promise of being a suitable p-type dopant, studies using a new Na source give us reason to believe that we are, for the first time, seeing the effects of incorporation of pure Na, and we have completed studies of Sb, finding it to be unsuitable as a p-dopant in ZnSe.

2.2.1 Na-Doped ZnSe on (100)GaAs

2.2.1.1 Na-Doped ZnSe: Growth and SIMS Analysis

Our previous Na-doping study indicated that Na seems to be a well-behaved acceptor impurity in ZnSe; the only problem we had with the Na_2Se source was inadvertent doping by donor impurities present in the dopant source.

During this quarter, we reexamined Na-doping using a new Na source, described elsewhere in this report. Since this source is unique for MBE growth, it was necessary to familiarize ourselves with the peculiarities of its use.

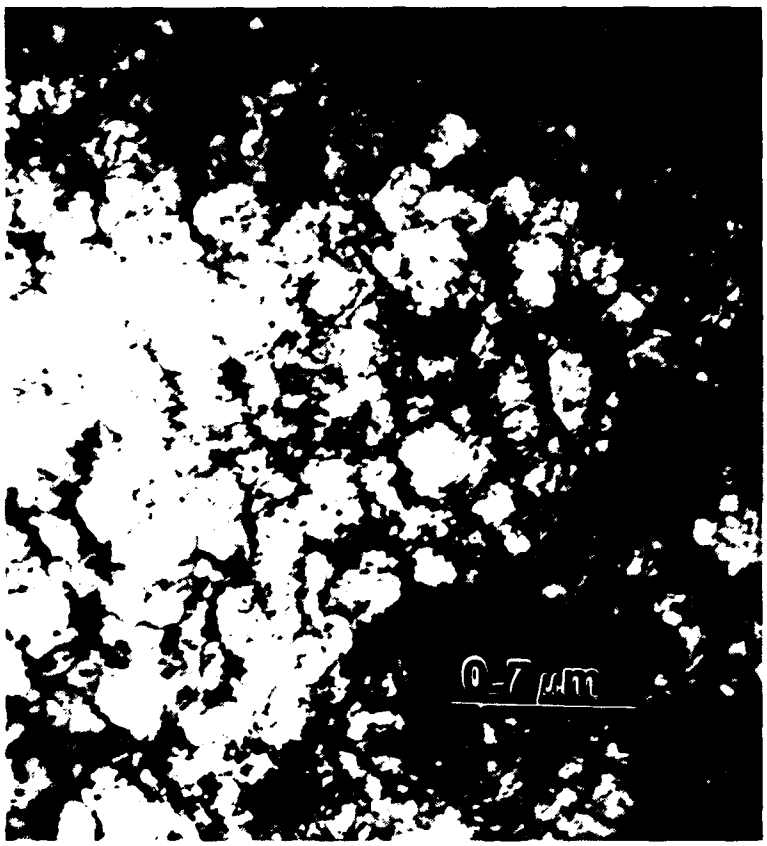

Figure 2-7. Conventional Transmission Electron Microscopy of ZnSe/(100) Ge Sample. Planar view, bright field image.

In particular, the relationship between the Na flux and the Na-cell temperature is not well established. It was found there is a break-in period for a new source to achieve a steady state. A dramatic increase in Na flux was observed during a source outgassing which lasted for several hours. Afterwards the Na flux was reasonably stable as measured by quadrupole mass spectrometer.

So far, eight Na-doped ZnSe samples have been grown under different conditions using the new Na source. Details of the growth conditions can be found in Table 2-1.

TABLE 2-1. Growth Conditions and SIMS Results for Na-Doped ZnSe Samples

Sample	BPR	T_g (°C)	Na Flux (arb units)	[Na] (10^{15} cm^{-3})
109	1:1	300	46	650,000
112	1:1	300	0.25	30
113	1:1	300	2	1000*
114	1:1	300	0.7	250
115	1:1	350	0.7	2.6
116	1:1	300	2	340*
118	1:1	350	4	5000*

* These samples show strong variations in Na content.

The SIMS determinations of Na concentrations in the Na-doped samples were performed as reported earlier (Quarterly Technical Progress Report No. 3), using a 1 micro ampere O_2^+ primary beam and detecting positive secondary ions. Na concentrations so determined are presented in Table 2-1. As in earlier attempts at Na-doping, it appears that the Na flux and growth temperature have strong effects on the Na incorporation.

One problem which was experienced with the current Na-doping technique is that the Na concentration in many doped samples was not a constant, but varied through the depth of the film and tended to be higher near the free surface of the film. Figure 2-8 shows an extreme example of this effect; here the Na concentration appears to jump abruptly from about $6 \times 10^{16}\,cm^{-3}$ deep in the sample to about $1 \times 10^{18}\ cm^{-3}$ near the surface. There are at least two possible causes for this type of profile. One possibility is that the Na is diffusing toward the free surface of the film. Another more likely explanation is that the Na flux coming from the source is not constant. This last possibility will be checked by monitoring the Na signal in the RGA before and after growth. (It cannot be monitored during growth because the filament in the RGA must be turned off to avoid contamination of the growing film.)

When it was discovered that the Na-doped films were high-resistivity n-type, SIMS studies to look for residual donors were begun. Preliminary positive secondary ion analyses revealed no significant contamination of the doped films.

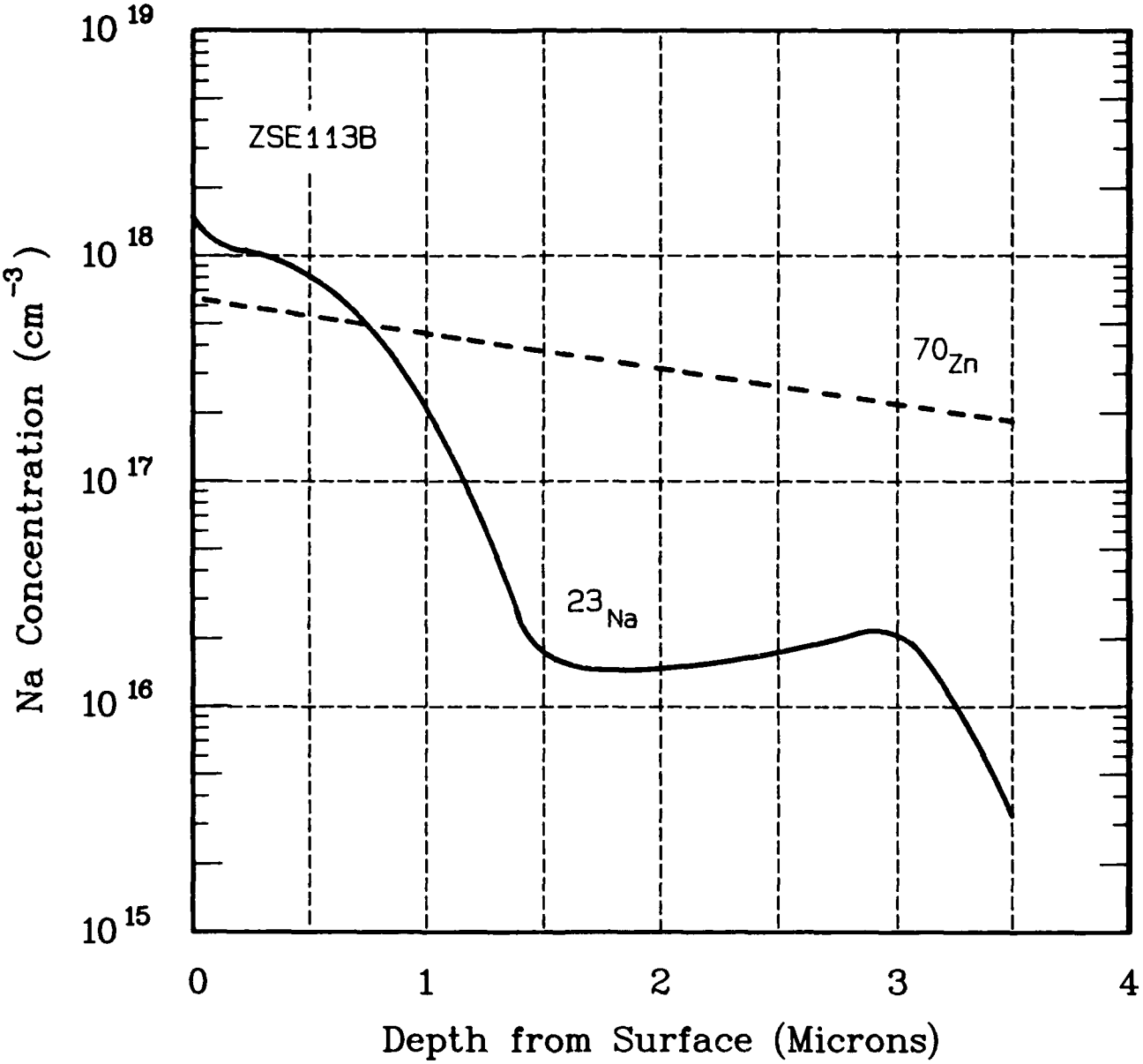

Figure 2-8. SIMS profile of a Na-doped film (ZSE113B) showing an anomalous variation of the ^{23}Na-concentration as a function of depth in the film. The ^{70}Zn reference signal (arbitrary units) is also shown for comparison.

2.2.1.2 Na-Doped ZnSe: Photoluminescence

In our Quarterly Technical Progress Report No. 4 we described our attempts at p-doping using Na from a Na_2Se source. There, we found that as the Na_2Se source temperature increased, the DBE peak intensity increased, as did the free carrier (electron) concentration. These results were interpreted to mean that donor-type impurities from contaminated Na_2Se source material were being incorporated into the film at a rate exceeding the incorporation of Na atoms. Since at that point neither we, nor anyone who had worked on Na-doping prior to that, had been looking at the incorporation of only Na, we were unable to predict the suitability of Na as a p-type dopant in ZnSe. In this quarter, we returned to Na-doping using the new alternate Na source described elsewhere in this report. The results, while quite different from those obtained for doping from Na_2Se and quite interesting in themselves, are not encouraging for the promotion of Na as the optimal acceptor atom for ZnSe.

SIMS measurements on the samples grown using the new Na source, shown graphically in Figure 2-9 indicate a monotonic increase in the incorporated Na concentration with increasing Na flux. (Electrical measurements, discussed later, show no increase in the carrier concentration in these samples.) This result alone represents a vast improvement over that seen using the Na_2Se compound as a dopant source where, for example, we saw essentially no change in the Na incorporation but a large increase in the (electron) carrier concentration as the Na_2Se cell temperature was increased from 375 to 500°C (see the data on samples ZSE68, 69, and 70 in Quarterly Report No. 4, Tables 2-3 and 2-4). Also, we have recently been able to incorporate Na at concentrations up to 6.5×10^{20} cm^{-3}, whereas we never incorporated more than 2×10^{17} cm^{-3} when using the Na_2Se source.

Figure 2-10 compares the PL spectra for samples ZSE72A and ZSE115A. Both were grown at T_G=350°C and BPR=1:1. ZSE72A was doped from the Na_2Se source and contains [Na] = 10×10^{15} cm^{-3}. ZSE115A was doped using the new Na source and contains [Na] = 2.6×10^{15} cm^{-3}. Whereas the spectrum for ZSE72A is dominated by the donor-bound-exciton peak I_x and contains a large DAP intensity, indicating a large concentration of donors, ZSE115A shows a dominant free exciton peak, some emission from acceptor-bound excitons, and a much weaker DAP intensity.

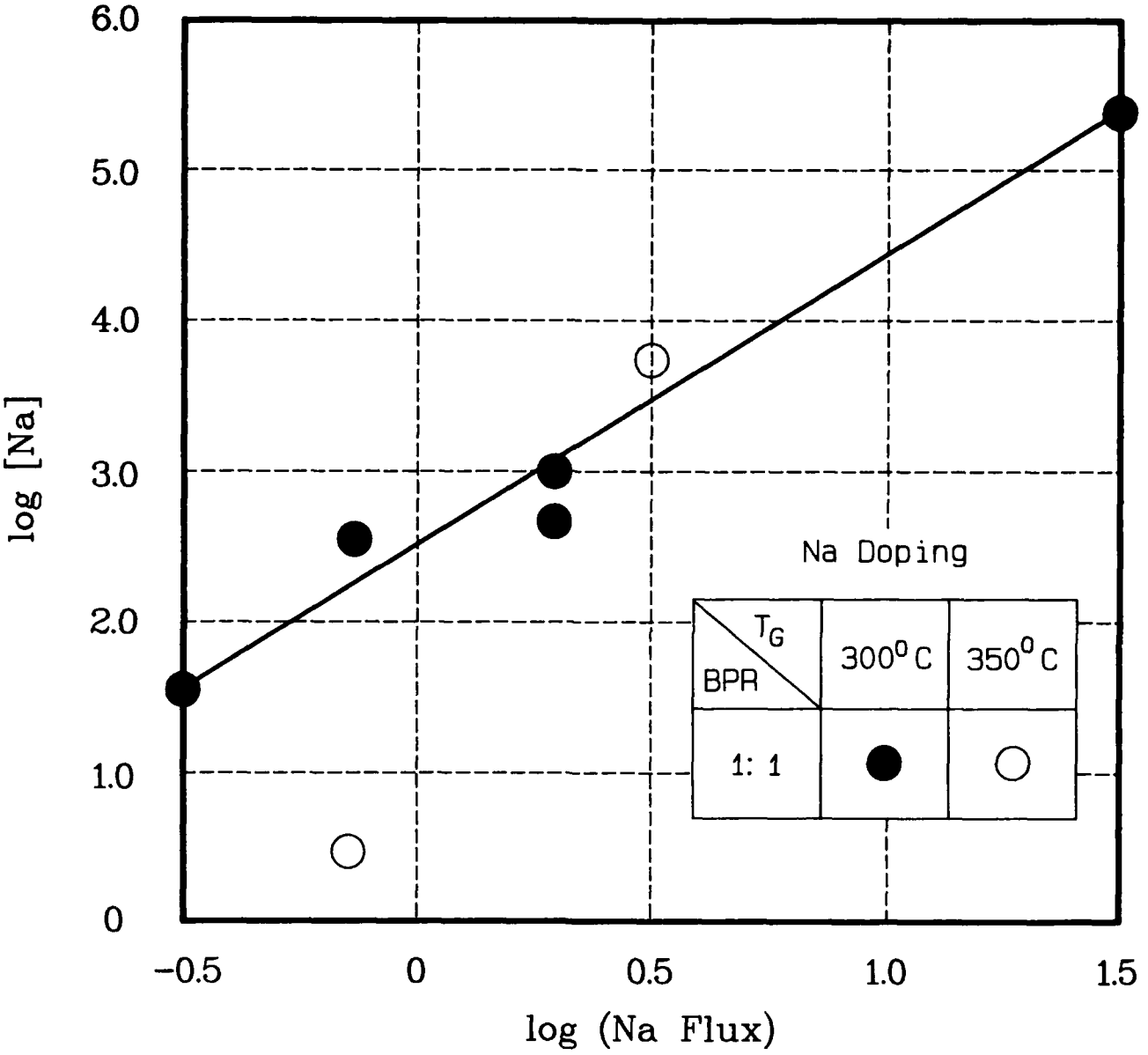

Figure 2-9. Log-log plot of the Na concentration, determined by SIMS, versus the Na flux (in arbitrary units), determined by the Na source temperature using the new Na source. Solid (open) circles represent films grown at a substrate temperature of 300 (350)°C.

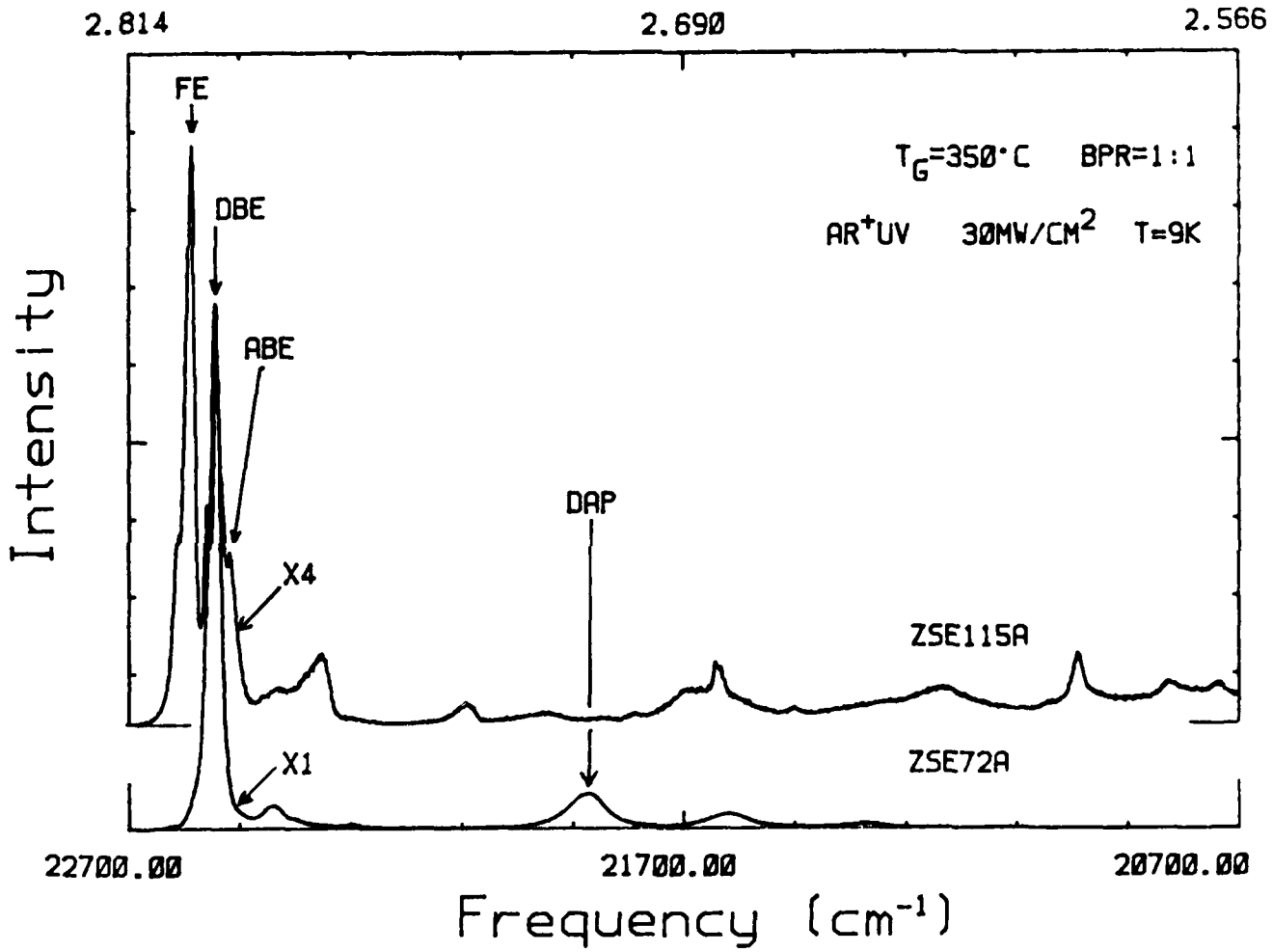

Figure 2-10. Near-Band-Edge PL spectra at 9K for Na-doped samples grown using Na_2Se source (ZSE72a; lower curve) and using the new "clean" Na source (ZSE115A; upper curve). The Na-concentration was approximately the same in the two samples.

It would appear that the new Na source is not emitting large quantities of undesired donor dopants as the Na_2Se source did, so that we are now testing, for the first time, the true effects of doping of ZnSe using pure Na.

Figure 2-11 shows the evolution of the PL spectrum as greater amounts of Na are incorporated into the lattice by increasing the Na flux. At low Na concentration (ZSE112A), we see a well-resolved DAP series beginning near 2.71 eV. The NBE emission in this case is dominated by the DBE peak rather than the free exciton as in Figure 2-10 because this sample was grown at T_G = 300°C rather than at 350°C as was the case for ZSE115A shown in Figure 2-10. As the concentration of Na increases, the DAP series disappears into a broad, structured feature centered near the position of the so-called Y_0 peak. For ZSE113A, with [Na] = 1 x 10^{18} cm^{-3}, the band near Y_0 dominates the spectrum; the NBE emission is almost entirely quenched. The Y_0 peak (typically with phonon overtones) has been associated with impurities at extended structural defects [8]. If this is so, the PL may be telling us that the Na is not being incorporated substitutionally at cation sites, but rather is accumulating near these extended defects. We know from our previous work on this project that the dislocations generated to relieve lattice mismatch strain at the ZnSe/GaAs interface should be confined to within 1 - 1.5 μm of the interface. As the Na-doped films in this study are all approximately 3 μm thick, we would not expect to find dislocation loops extending to the near-surface regions probed in the PL experiment. Perhaps the Na itself is inducing structural defects into the lattice. If so, and if no combination of growth parameters could be found which would alleviate this problem, then Na would be unsuitable for p-doping of ZnSe. We are performing X-ray DCRC measurements and obtaining TEM photomicrographs of these Na-doped films to look for evidence of the extended defects predicted by the appearance of the Y_0 band.

Another possibility, of course, is that Na in dilute concentrations forms a shallow acceptor level, but at higher concentrations it forms a deep level, in a way reminiscent of the behavior of P (see Section 2.2.3 of our Quarterly Report No. 4). The deep level in this case would be only about 200 meV deep in this case, if we assume that the band near Y_0 is the DAP spectrum for this deep acceptor and a typical shallow donor.

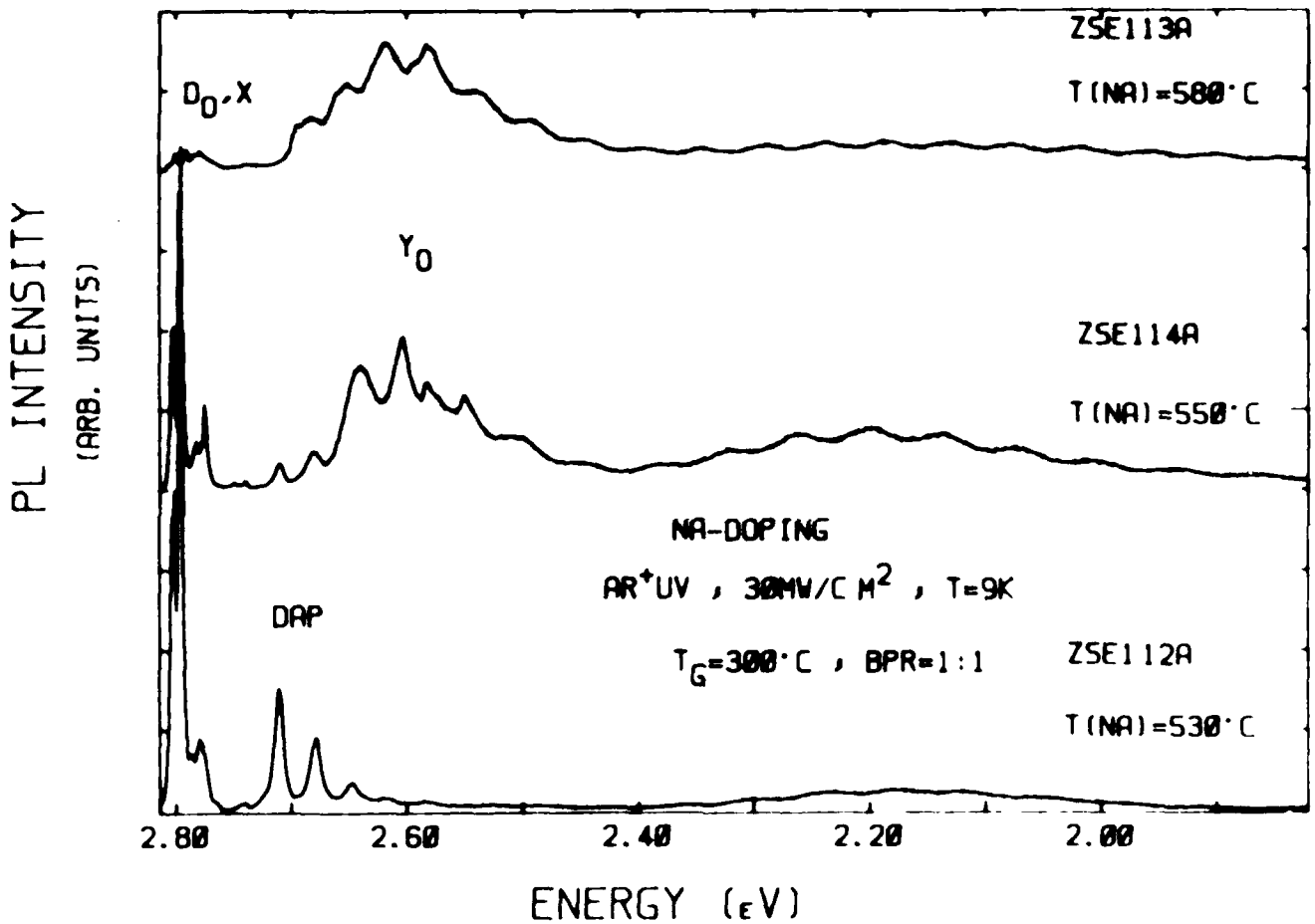

Figure 2-11. 9K PL spectra for three Na doped samples. The Na concentration was increased in this series by increasing the Na [illegible] temperature. Data for these samples may be found in [illegible]

The deep level in the P case, on the other hand, was 600-800 meV deep. If this explanation or the one given in the previous paragraph proves to hold up, the results in either case would be discouraging for the prospect of using Na as a p-dopant in ZnSe.

2.2.1.3 Na-Doped ZnSe: Electrical Characterization

Eleven samples (ZSE108A - ZSE118A) were grown to investigate the effects of sodium doping. Three of these samples (ZSE108A, ZSE110A, and ZSE117A) were not doped and ZSE111A was grown only for diagnostics; the remaining seven samples were doped with sodium. Electrical measurements were attempted on all samples except ZSE111A.

All three undoped samples were found to be n-type. The room temperature carrier concentrations measured for ZSE108A, ZSE110A, and ZSE117A were 9.1×10^{15}, 6.1×10^{15}, and 1.4×10^{14} cm^{-3}, respectively. Notice that the carrier concentration is decreasing as more samples are grown. One possible explanation for this is that one of the sources was originally contaminated and is slowly being "cleaned up".

The only Na-doped sample on which electrical measurements could be made was ZSE112A which was grown with an extremely small Na flux. This sample was found to be n-type with a room temperature carrier concentration of 4.8×10^{15} cm^{-3}. SIMS measurements on this sample (see Table 2-1) indicate a Na concentration of 3×10^{16} cm^{-3}. It appears that, while the incorporated Na atoms have not compensated the residual donors to any great extent, the Na source itself is not contributing a large density of extrinsic donors, as was the case for the Na_2Se source. No electrical measurements could be made on any of the other Na-doped samples. When measurements were attempted (with both Au and In contacts), it was found that the resistivities of the epilayers were so great that the current passing through the substrate was much greater than the current through the epilayer itself.

2.2.1.4 Na-Doping Summary

ZnSe samples doped using the new Na sources were found to be high resistivity. This seems to represent an improvement over the Na-doped samples grown earlier, which were n-type and of lower resistivity with carrier concentration of above 1 x 10^{17} cm^{-3}. However, the new samples are found to have PL spectra which are fundamentally different from the early samples, and which show strong evidence of structural defects. This may indicate that sufficient doping with pure Na results in the production of structural defects and degraded material. It is possible that the PL evidence of defects through the enhancement of the Y peak was not observed in earlier work due to contamination introduced with the Na dopant, and the resultant dominance of the donor-bound exciton.

In summary, Na now appears to be less promising than Li as an acceptor dopant. However, further work is necessary in order to verify the detrimental behavior of Na.

2.2.2 Sb-Doped ZnSe on (100) GaAs

2.2.2.1 Sb-Doped ZnSe: Growth and SIMS Analysis

Some preliminary results on Sb-doping of ZnSe were reported in the Quarterly Technical Progress Report No. 4. During this quarter a more detailed study was undertaken into the growth parameter dependence of Sb incorporation into the ZnSe lattice. Sb incorporation was studied as functions of substrate temperature, T_s, Sb cell temperature, T_{Sb}, and beam pressure ratio, P_{Zn}/P_{Se}. The layers in this study were all grown on conducting GaAs substrates in order to reduce charging effects in the SIMS measurements.

Several layers were grown at a fixed T_{Sb}, namely 600°C and a beam pressure ratio of unity using different substrate temperatures in the range 250 to 330 C.

The measured Sb concentrations by SIMS as a function of T_G are shown in Figure 2-12 together with the estimated incorporation coefficients deduced from beam pressure measurements of Sb flux. As can be seen from the figure the Sb incorporation coefficient varies from ~ 10^{-2} to ~ 1 over the T_{SUB} range 300 to 250°C.

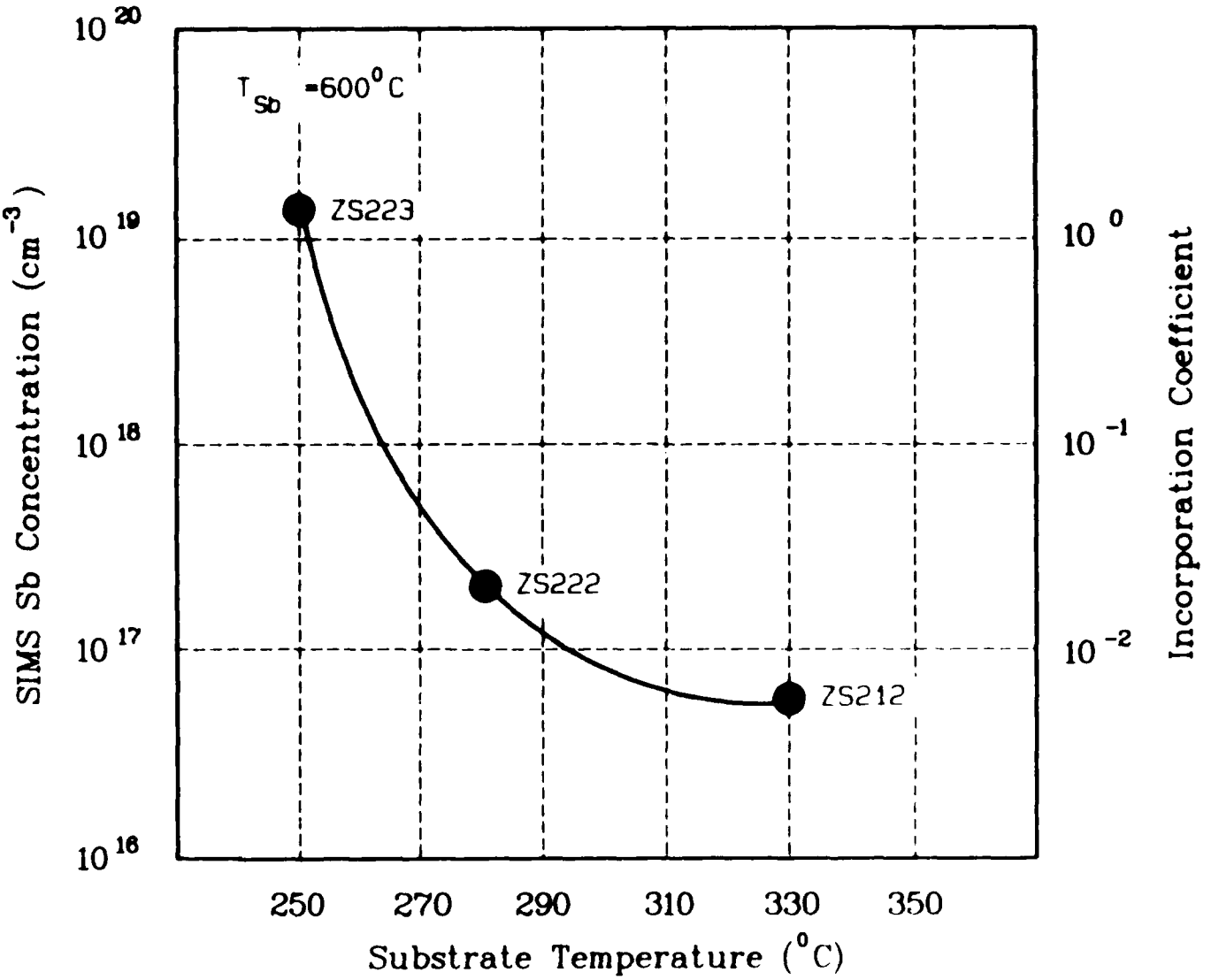

Figure 2-12. Sb-concentrations, as determined by SIMS measurements, as a function of the substrate temperature during growth. For all of these samples the Sb-source temperature was 600°C.

Since a T_G of 330°C was shown previously to be 'optimum' for ZnSe growth, a series of layers was grown at this T_{SUB} but using various Sb cell temperatures in the range 550 to 800°C (the Zn/Se ratio was ~ 1). The measured Sb concentrations in the layers are plotted as a function of T_{Sb} in Figure 2-13. Also shown in Figure 2-13 are the Sb beam pressures measured as a function of T_{Sb} at the substrate location. The dashed line represents an extrapolation of the beam pressure curve to lower pressures, 10^{-9} mbar being the lowest pressure measurable with reasonable accuracy. As can be seen from the figure, the measured Sb concentrations follow the Sb pressure/temperature curve quite closely indicating the incorporation coefficient to remain essentially constant with increasing Sb flux at ~ 10^{-2} for T_{SUB} = 330°C. Sb concentrations in the range, mid-10^{16} to mid-10^{19} cm^{-3} were obtained. It should be noted that the layers with Sb concentrations in the 10^{19} cm^{-3} range exhibited RHEED patterns which were indicative of mixed polycrystalline/single crystalline material. An example of such a RHEED pattern is shown in Figure 2-14(a). On the other hand, for Sb concentrations < 10^{19} cm^{-3}, RHEED indicated a smooth (2 x 1) surface reconstructed single crystal pattern as illustrated in Figure 2-14(b). In fact, in certain cases the 1/2-order diffraction lines only became apparent on opening the Sb-shutter.

Finally, from SIMS analysis it is apparent that the use of large Zn to Se ratios did not result in enhanced Sb incorporation as one might have expected. Layers ZS220 and ZS221, for example, were grown at a T_G of 330°C and a T_{Sb} of 650°C but with different beam pressure ratios, namely 1:1 and 1:4, respectively. SIMS analysis in fact, indicated layer ZS221 to have a significantly lower Sb concentration than ZS220.

Although it appears that Sb can be incorporated quite readily in ZnSe by MBE to concentrations in excess of 10^{19} cm^{-3} (single-crystal limit, $\sim 10^{20}$ cm^{-3}), the element does not seem to substitute simply for Se atoms in the ZnSe lattice. There seems to be no evidence for an acceptor bound exciton in the photoluminescence spectra recorded from Sb-doped ZnSe layers which would indicate the presence of an acceptor level in the band gap. We therefore conclude at this stage that p-type ZnSe apparently cannot be obtained by MBE doping with Sb in the form of [illegible]

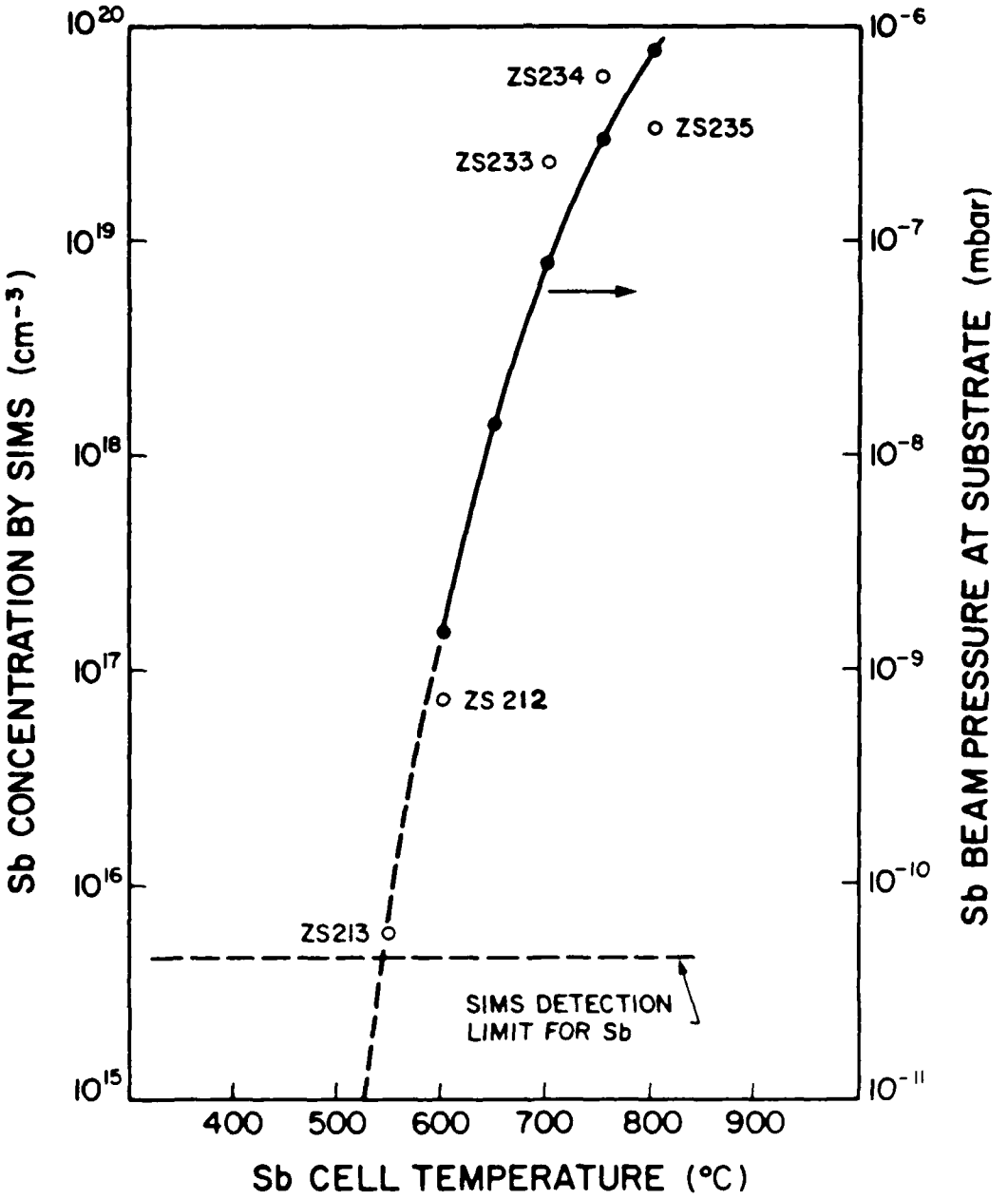

Figure 2-13. Sb-concentrations, as determined by SIMS measurements, versus Sb-source temperature. For all of these samples, the substrate temperature during growth was 330°C.

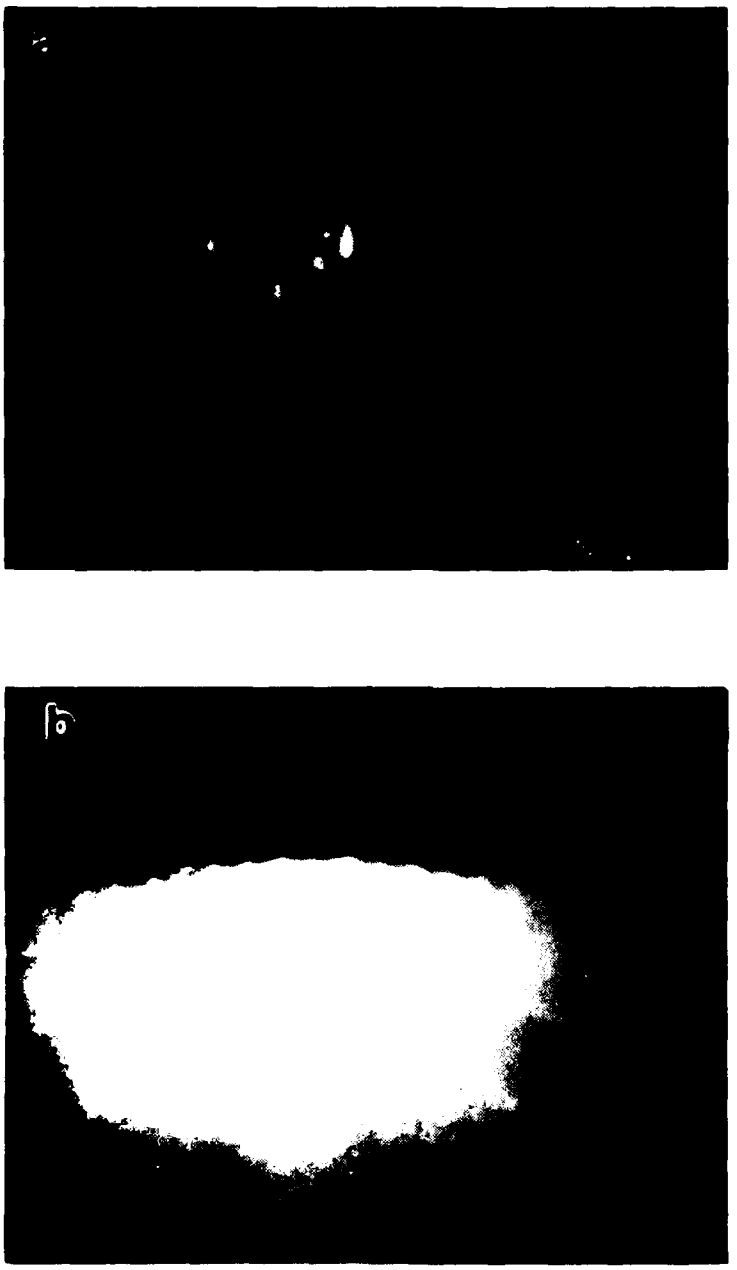

Figure 2-14. RHEED patterns recorded in the [1$\bar{1}$0] azimuth during growth of Sb-doped ZnSe. (a) Spotty pattern, indicative of mixed polycrystalline/single crystal material, when the Sb concentration was approximately 10^{19} cm^{-3}. (b) Smooth (2 x 1) surface reconstructed single crystal pattern for Sb concentration less than 10^{19} cm^{-3}.

2.2.2.2 Sb-Doped ZnSe: Photoluminescence

In Quarterly Technical Progress Report No. 4, preliminary results of the low-temperature PL measurements indicated the presence of a peak at 445.4 nm which may be attributed to an acceptor-bound exciton at a shallow Sb acceptor level. However, we cautioned that this peak was very close to the I_1^{Deep} peak commonly observed at 2.783 eV and attributed to Cu and/or defects. In subsequent studies which we report on here, there was no evidence of a strong peak at 445.4 nm for ZnSe grown under different conditions of Sb flux, substrate temperatures, and beam pressure ratios. At this time we therefore attribute the 445.4 nm peak observed earlier to I_1^{Deep}.

In order to determine the effect of Sb-doping on the PL spectrum of layers grown at "optimum" conditions (namely, T_G = 330°C and BPR of unity), ZS-219 was grown with the Sb cell off and ZS-220 with the Sb cell temperature at 600°C. Figures 2-15(a) and 2-15(b) show that the excitonic emission in the doped sample (ZS-220) is about a factor of 13 times larger than that of ZS-219. In both cases the deep-level emission relative to the excitonic emission is very small being about 300 times smaller for ZS-219 and 740 times for ZS-220. Although the D-A pair emission is relatively strong in the Sb-doped sample it is quite weak related to the excitonic emission even though SIMS measurements show an Sb concentration greater than $10^{16}\,cm^{-3}$. Furthermore, the D-A pair emission is also present in the spectrum of the unintentionally doped material albeit much weaker. Figures 2-15(c) and 2-15(d) which show the excitonic emission spectra of the two layers are very similar although different in absolute amplitudes and indicate the absence of a new emission peak which may be associated with Sb doping. There is, therefore, no clear evidence that Sb incorporation gives rise to a shallow acceptor level in ZnSe. However, the results are interesting in that they suggest that at the "optimum" growth conditions material of better quality, as measured by 4.2K PL spectroscopy, is obtained when the layer is grown in the presence of an Sb flux.

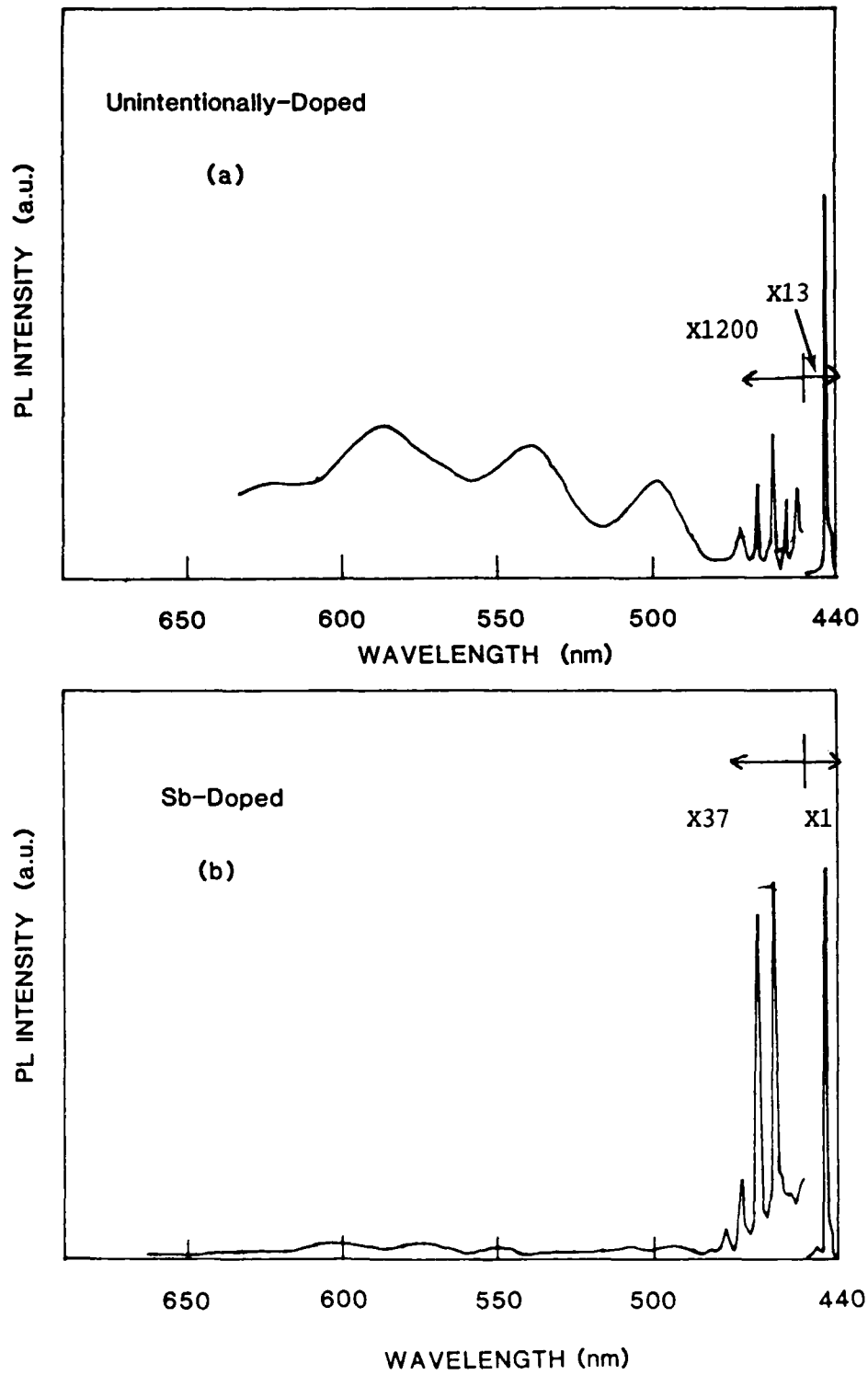

Figure 2-15. 4.2K PL spectra for two ZnSe films grown at T_g = 330°C and BPR = 1:1, using Sb-cell temperatures of (a) ambient (i.e., Sb-source turned off) and (b) 600°C.

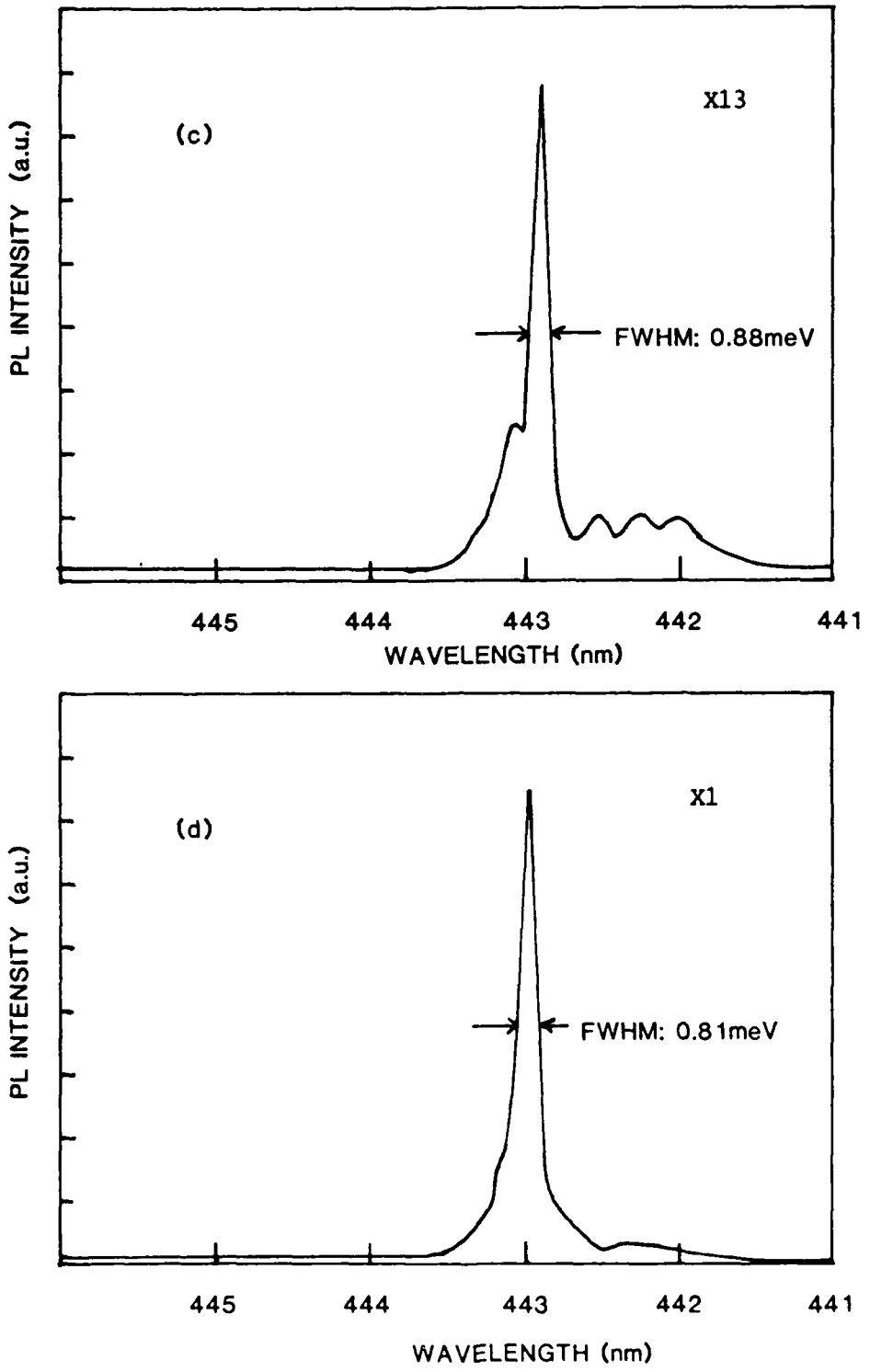

Figure 2-15. The NBE PL spectra for these two films are shown in (c) and (d), respectively. No evidence for an acceptor-related feature is seen in (d).

In order to determine the effect of substrate temperature on Sb incorporation, as determined by the 4.2K PL measurements, several layers were grown at a fixed Sb-cell temperature (660°C) and a beam pressure ratio of unity. The PL spectra shown in Figure 2-16 demonstrate a marked reduction in overall quality of the PL spectra with decreasing T_{SUB}. This is especially evident for the excitonic emission which decreased by a factor of about 1,540 in decreasing T_G from 330°C to 280°C. At 250°C the ZnSe is practically optically dead. In none of the spectra is there any evidence of an increasing emission peak associated with the increasing Sb even though SIMS results (described in Section 2.2.2.1) show an increase in Sb incorporation of more than two orders of magnitude with a decrease in T_{SUB} from 330°C to 250°C. Note, however, that D-A pair no-phonon peak is present at about 460 nm; assuming a shallow donor level ($E_D \simeq 28$ meV), the acceptor level will be shallow. Nonetheless, it should be pointed out that D-A pair emission is present even in the unintentionally doped ZnSe grown under identical conditions albeit much weaker. These results suggest, as indicated above, that if Sb is being incorporated at substitutional sites the level(s) associated with it is (are) deep. It is also possible that the Sb atoms are being incorporated at defects such as dislocations or are forming associates involving two or more atoms with deep energy levels.

2.2.2.3 Laser-Enhanced Sb-Doping of ZnSe: Growth and Photoluminescence

We report here on preliminary results of a series of experiments which were begun in an attempt to determine the effect of laser excitation of the layer during growth on the Sb incorporation. This work was motivated by the successes at North Carolina State University on laser-enhanced Sb and In incorporation in MBE-grown CdTe. An interesting set of results was obtained using the 465 nm line of the Ar^+ laser. As reported above, ZS-223 growth at 250°C with a BPR of unity and with the Sb-cell temperature of 600°C (monitored) was found by PL to be practically optically dead. However, for a layer (ZS-228) grown under identical conditions but irradiated with the laser light during growth, there was dramatic improvement in the PL characteristics and, hence, the quality of the ZnSe layer as shown in Figure 2-17. In addition, the layer showed excellent 1/2-order surface reconstruction in the RHEED pattern.

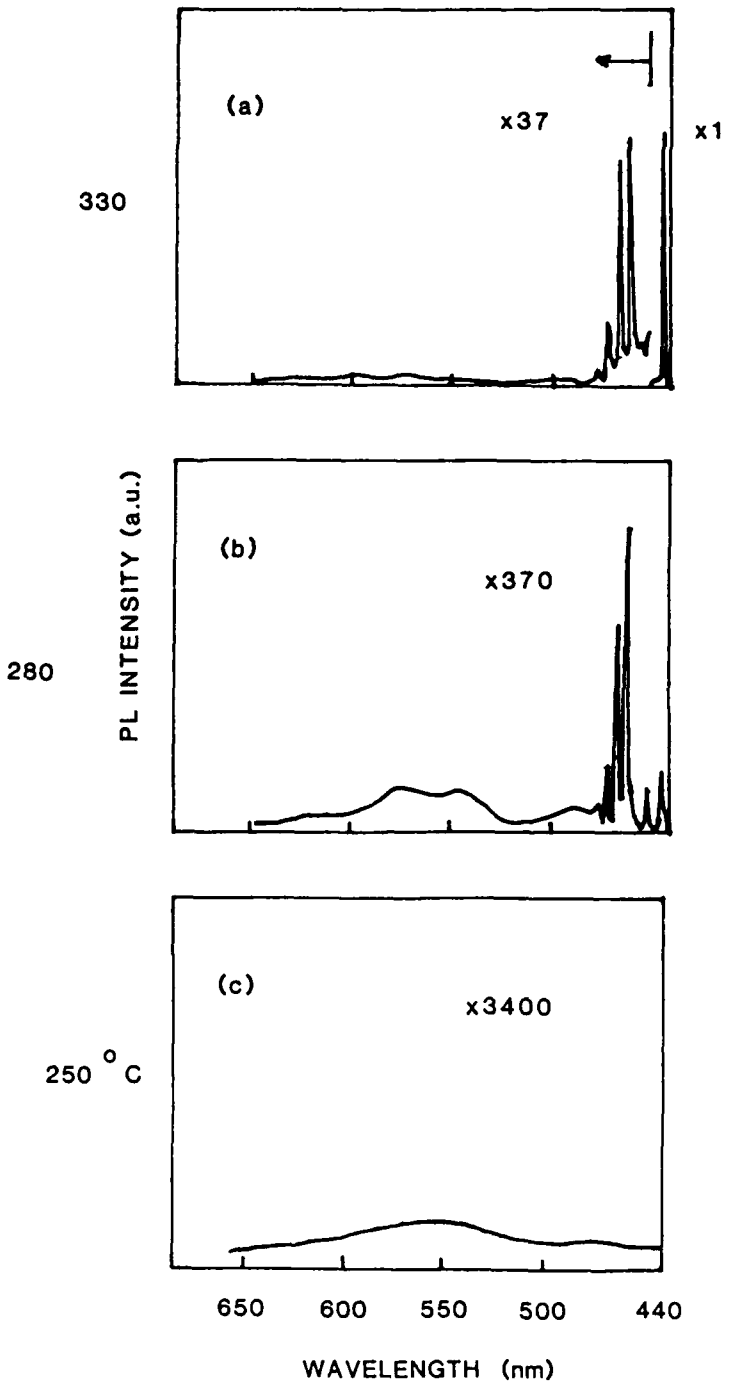

Figure 2-16. 4.2K PL spectra for three Sb-doped ZnSe films grown using BPR = 1:1 and Sb-source temperature of 600°C (monitored). The Sb-concentrations were varied by changing the substrate temperature during growth: T_{SUB} = (a) 330°C, (b) 280°C, (c) 250°C.

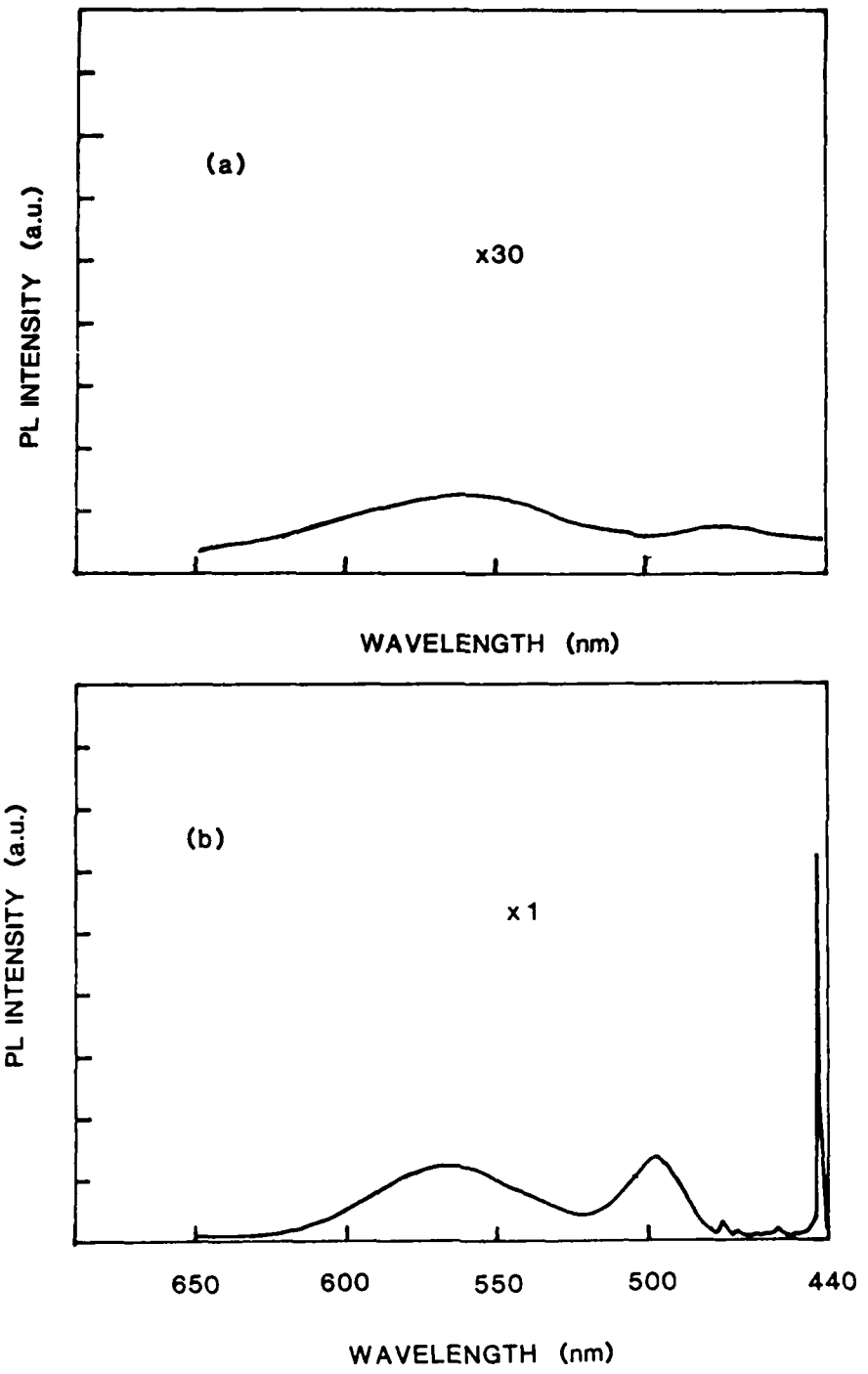

Figure 2-17. 4.2K PL spectra for two Sb-doped ZnSe films grown under identical conditions (T_G = 250°C, BPR = 1:1, T_{Sb} = 600°C), but (a) was grown without laser illumination and (b) with laser illumination of the substrate during growth.

However, the 4.2K PL spectrum of the layer grown with laser excitation did not reveal any emission peaks which may be associated with Sb incorporation.

An experiment was then performed to determine the effect of the laser light on layers grown under the same conditions s that of ZS-223 and ZS-228 but without the presence of the Sb flux. Figure 2-18 shows there is virtually no difference in the 4.2K PL spectra of ZS-230 grown with the laser and ZS-231 grown without the laser. In addition, the excitonic linewidths, indicated in Figures 2-18(c) and (d) are similar to that of ZS-219 (~ 0.81 meV) which was grown at 330°C without Sb doping. These results suggest that decreasing T_G has little effect on the quality of layers not doped with Sb as determined by low-temperature PL spectroscopy in the range $330°C \geq T_G \geq 250°C$. However, with increasing Sb incorporation (which is high at low growth temperatures) there is a marked reduction in the layer quality. Furthermore, the quality of the layers grown at 250°C with high Sb fluxes can be significantly improved by use of the 465 nm line of the Ar^+ laser at a power density of 100 mW/cm^{-2}.

The observation that unintentionally-doped ZnSe layers grown at 250°C are of similar quality to layers grown at 330°C is contrary to our earlier observations and is at present puzzling.

2.2.3 Li-Doped ZnSe on (100)GaAs

2.2.3.1 Li-Doped ZnSe: Growth

Lithium has been reported to be an acceptor impurity in ZnSe if it is substitutionally incorporated on a Zn site, but a shallow donor will be formed if Li goes to an interstitial site. Previous attempts to obtain high conductivity p-type ZnSe epitaxial films by Li-doping have met with some success. Nishizawa [9] reported the formation of p-n junctions in ZnSe, using a vapor-transport technique to grow the crystals and doping with Li acceptors. More recently, encouraging results were reported by a group headed by Professor Kukimoto of Tokyo Inst. of Tech., Japan [10]. They claimed that p-type ZnSe with a hole concentration from 10^{16} to 10^{18} cm^{-3} and a mobility of 40 cm^2/V-sec has been achieved in their MOCVD-grown ZnSe films. They used Li_2N and Li_2S compounds as their doping sources. (Recent informal reports from Japan have cast some doubt on the validity of these results.)

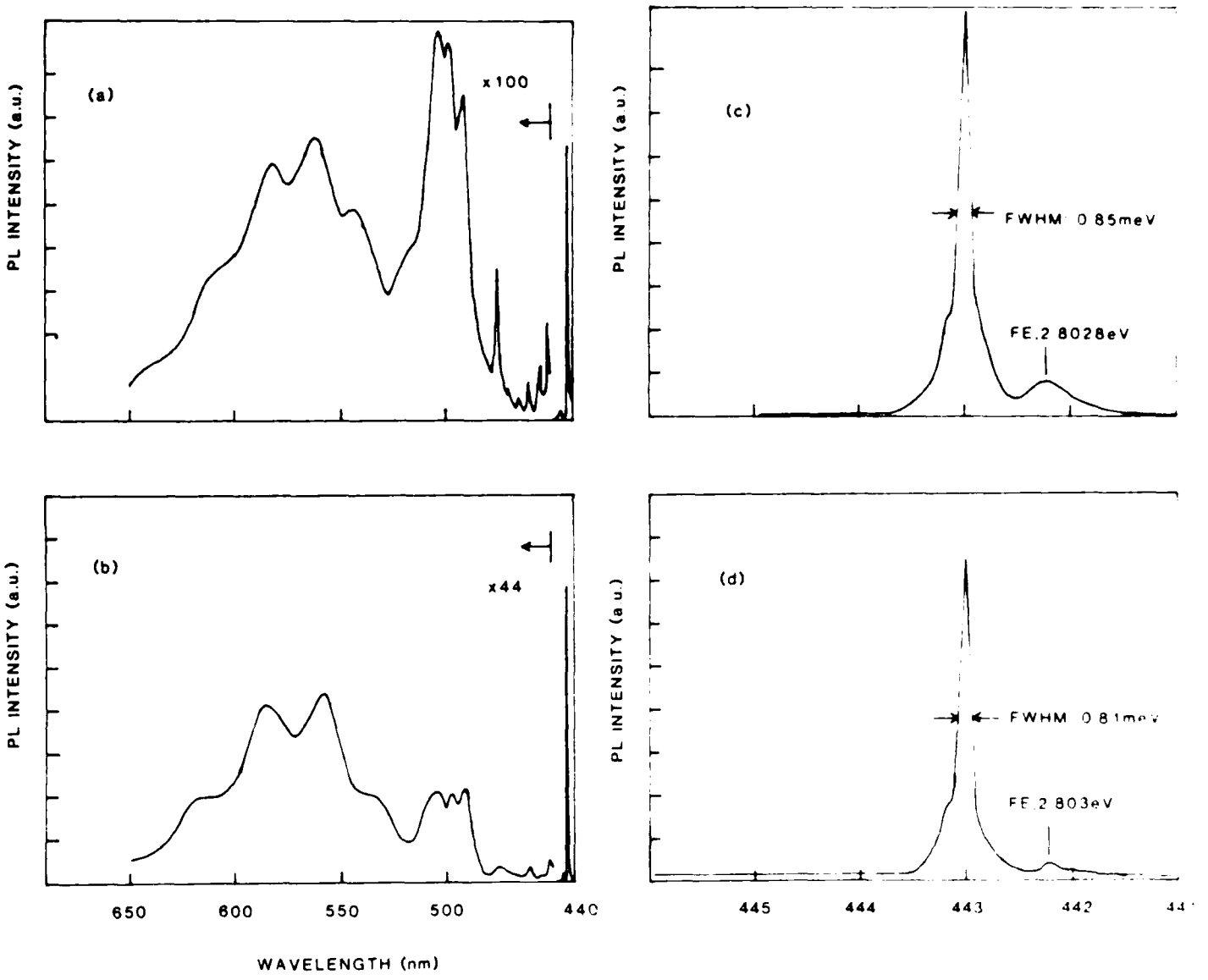

Figure 2-18. 4.2K PL spectra for two not-intentionally-doped ZnSe films grown at T_G = 330°C and BPR = 1:1, demonstrating that laser illumination during growth has very little effect on these undoped films. (a) and (c) grown with laser illumination; (b) and (d) grown without laser illumination.

We have used for our Li-doping studies the Li source described elsewhere in this report. After extended bakeout of the source, we examined the species effusing from the source oven using the quadrupole mass analyzer (QMA). We have found that K and Na are the major contaminants in the source flux; their QMA signals were even larger than those of the Li, presumably because of their larger vapor pressures. Some trace amounts of F were also present, but this disappeared after heating the source for several hours. After a more prolonged (overnight) bakeout, the Na and K fluxes were no longer detectable on the QMA. We note, however, that the QMA could not detect contaminants at the part-per-million level.

In this doping series, eight Li-doped ZnSe specimens were grown under various condition before we ran out of Zn. The details of growth condition for each sample will be shown with the SIMS results. Since Li can be either an acceptor or a donor depending upon the site it occupies, the main emphasis of this study is to understand the effect of growth condition on the incorporation of Li in the MBE growth of ZnSe. This was achieved by using the same Li flux (3 units) and varying either the growth temperature or BPR. A very impressive PL spectrum was also observed from one of the Li-doped specimens grown at higher growth temperature (350°C). Samples doped with higher Li concentration (30 units) had a hazy surface and their PL spectra were generally worse than those doped with less Li. These important observations will be further discussed in the next section.

2.2.3.2 Li-Doping: SIMS Analysis

The Li concentrations in Li-doped samples were determined by secondary ion mass spectrometry (SIMS), using a primary ion beam of 1 micro ampere O_2^+ and positive secondary ion detection. Results were quantified using a standard consisting of a Li ion-implanted ZnSe epilayer. The detection limit for Li was about 1×10^{14} cm^{-3} under the conditions used here. Li concentrations determined in this way are presented in Table 2-2.

TABLE 2-2. Growth Conditions and SIMS Results for Li-Doped ZnSe Samples

Sample	BPR	T_g (°C)	Li Flux (arb units)	[Li](10^{15} cm^{-3})
100	1:1	300	3	40
101	1:1	300	3	120
102	1/4:1	300	3	150
103	1/4:1	300	30	320
104	1:1	300	30	2600
105	1:1	250	3	1000
106	1:1	350	3	120
107	1:1	350	30	560

As can be seen from Table 2-2, Li concentrations in excess of 2×10^{18} cm^{-3} were easily obtained. Furthermore, it is apparent that not only the Li flux and the growth temperature, but also the Zn:Se BPR, control the Li concentration.

Because of the low hole concentrations observed in electrical measurements, SIMS analyses of contamination in the Li-doped samples have begun. Positive secondary ion mass spectra have revealed a wide variety of contaminants whose concentrations are apparently enhanced by the Li-doping. Species present include: Na, K, Rb, Ca, Sr, Mn, Fe, Ni, Cu, Si, Ga, and I. All of these species have also been detected in the dopant source material. Efforts to devise methods to reduce contamination during Li doping are currently underway.

2.2.3.3 Li-Doped ZnSe: Photoluminescence

As discussed elsewhere in this report, our initial efforts at Li-doping have met with some success. Photoluminescence (PL) measurements on these Li-doped samples have been most interesting. Figure 2-19 shows the near-band-edge and edge emission regions for an undoped sample (ZSE99A; T_G = 300°C, BPR = 1:1) and a lightly Li-doped sample (ZSE106A; T_G = 350°C, BPR=1:1, Li flux=3). Whereas the PL from the undoped sample is weak and is

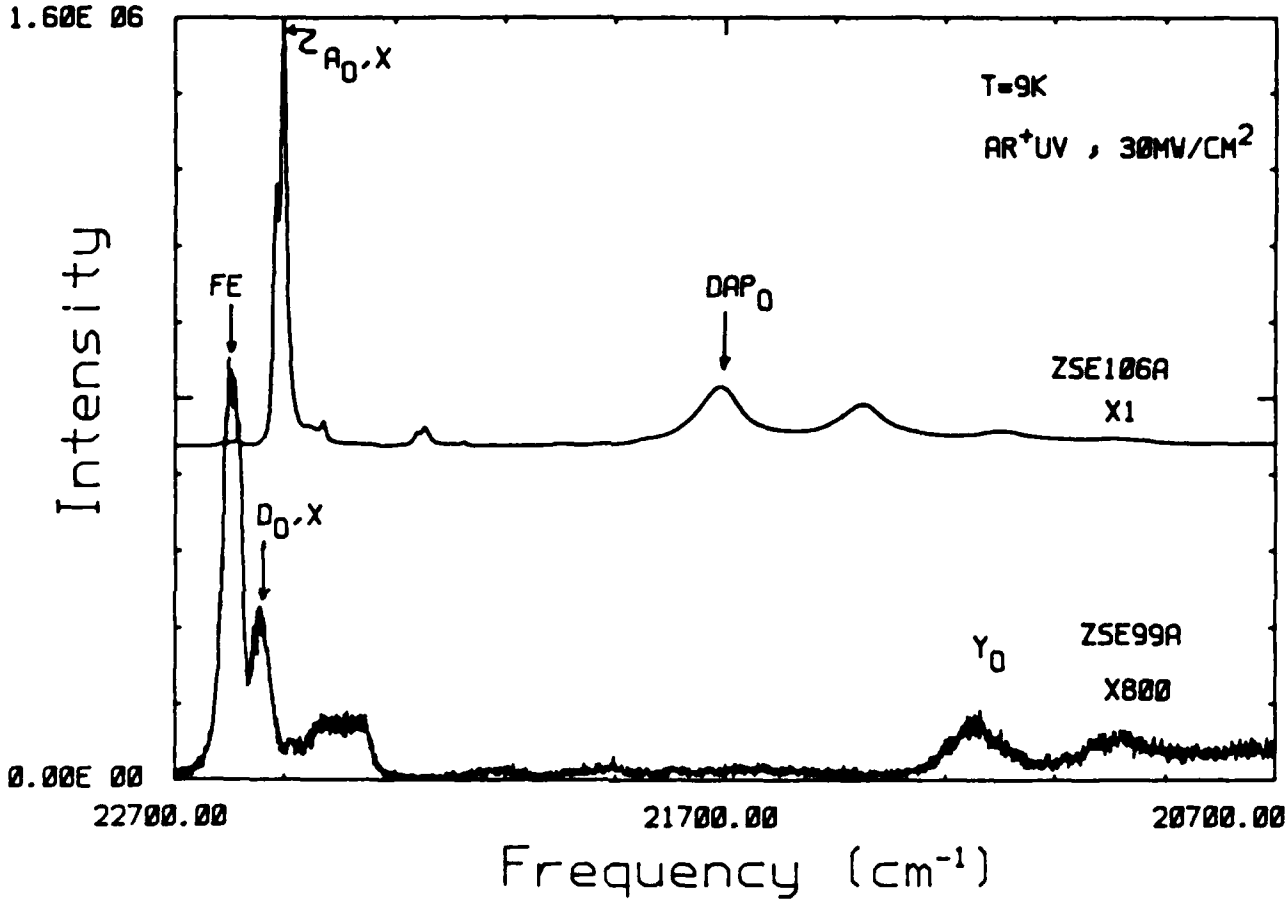

Figure 2-19. A comparison of the 9K PL spectra for two films grown using similar growth conditions but with and without Li flux. (Lower curve) ZSE99A: T_G = 300°C, BPR = 1:1. (Upper curve) ZSE106A: T_G = 350°C, BPR = 1:1, Li-Flux = 3 (in arbitrary units). The dominant acceptor-bound-exciton emission, and the absence of any donor-bound-exciton emission in the spectrum of the Li-doped sample is particularly noteworthy.

dominated by the free exciton (FE) and donor-bound exciton (DBE) emissions, the strong PL from the Li-doped sample is dominated by the acceptor-bound exciton (ABE) peak and also shows some donor-acceptor pair (DAP) emission. These measurements represent the first report of dominant ABE emission in alkali-doped ZnSe. (Our 3M Canada lab, as part of this project, has demonstrated dominant ABE emission from a N-doped film [11]; similar results with N have been reported recently from Matsushita [12]).

Clear trends could be found in the PL measurements made on Li-doped ZnSe films, although the interpretation of these measurements presents some ambiguities. For example, Figure 2-20 demonstrates that the intensity of the I_1^{Li} acceptor-bound exciton peak increases monotonically with increasing growth temperature, while the donor-acceptor pair emission intensity saturates at around 300°C, and the deep level (DL) emission actually decreases slightly at the higher temperatures. These trends are the same for both low and high incident Li flux. Taken alone, the I_1 data would indicate that more Li was being incorporated as the growth temperature increased, and the saturation of the DAP would indicate that the number of incorporated acceptors had overtaken the residual donors. In fact, these conclusions are in contradiction to the SIMS results which show (see Figure 2-21) that the Li concentration in the films actually decreases as the growth temperature increases; this is closer to the behavior that would be expected based on simple considerations of reabsorption. Perhaps the PL results are telling us that, with increasing growth temperature, the Li is increasingly incorporated on the correct sites; i.e., substituting on the Zn sites.

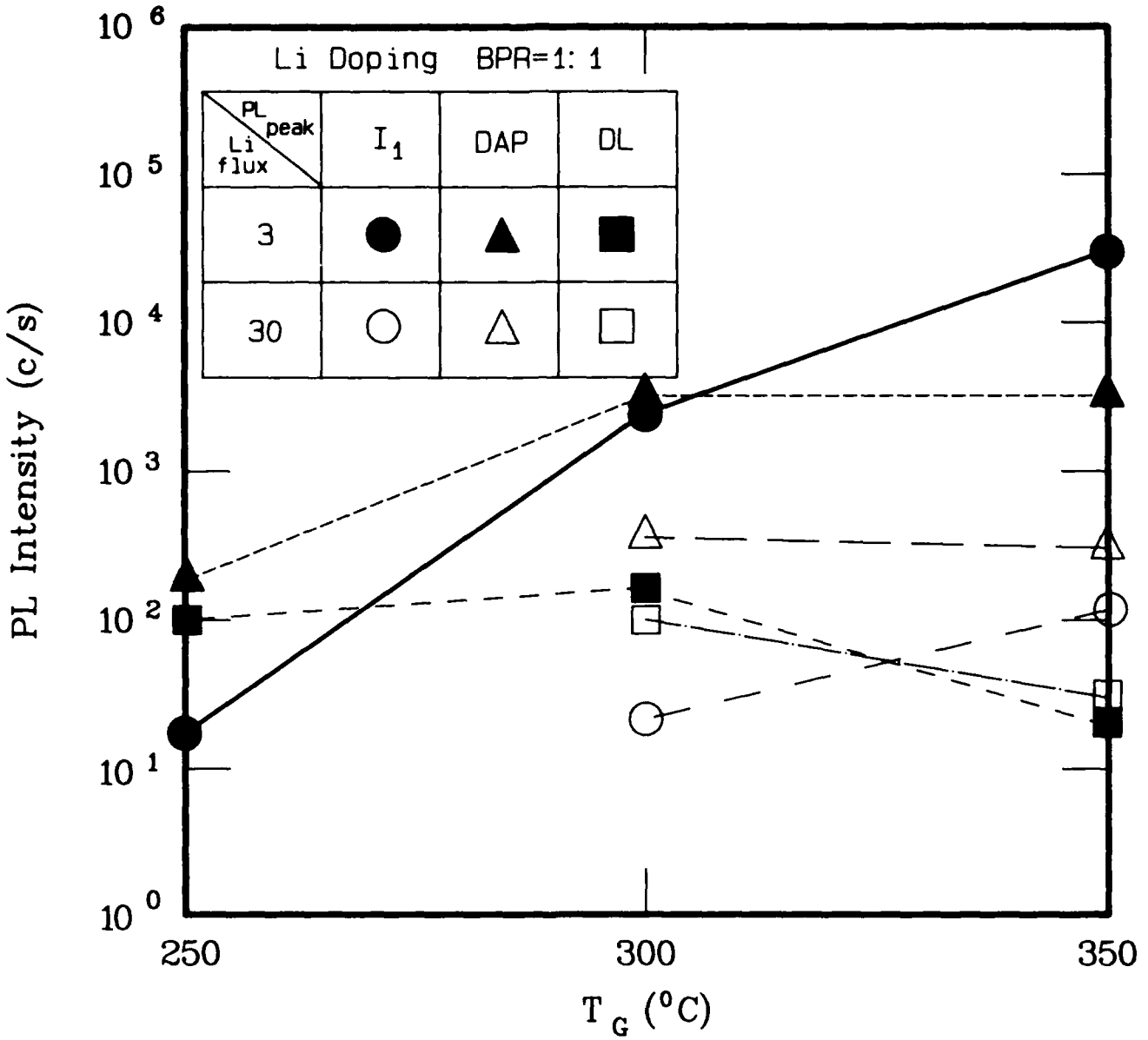

Figure 2-20. PL intensity for three different PL features versus substrate temperature during growth. Circles: acceptor-bound exciton peak. Triangles: donor-acceptor pair emission peak. Squares: deep-level emission. Solid (open) symbols represent data for Li-fluxes of 3(30), where the Li-flux is given in arbitrary units.

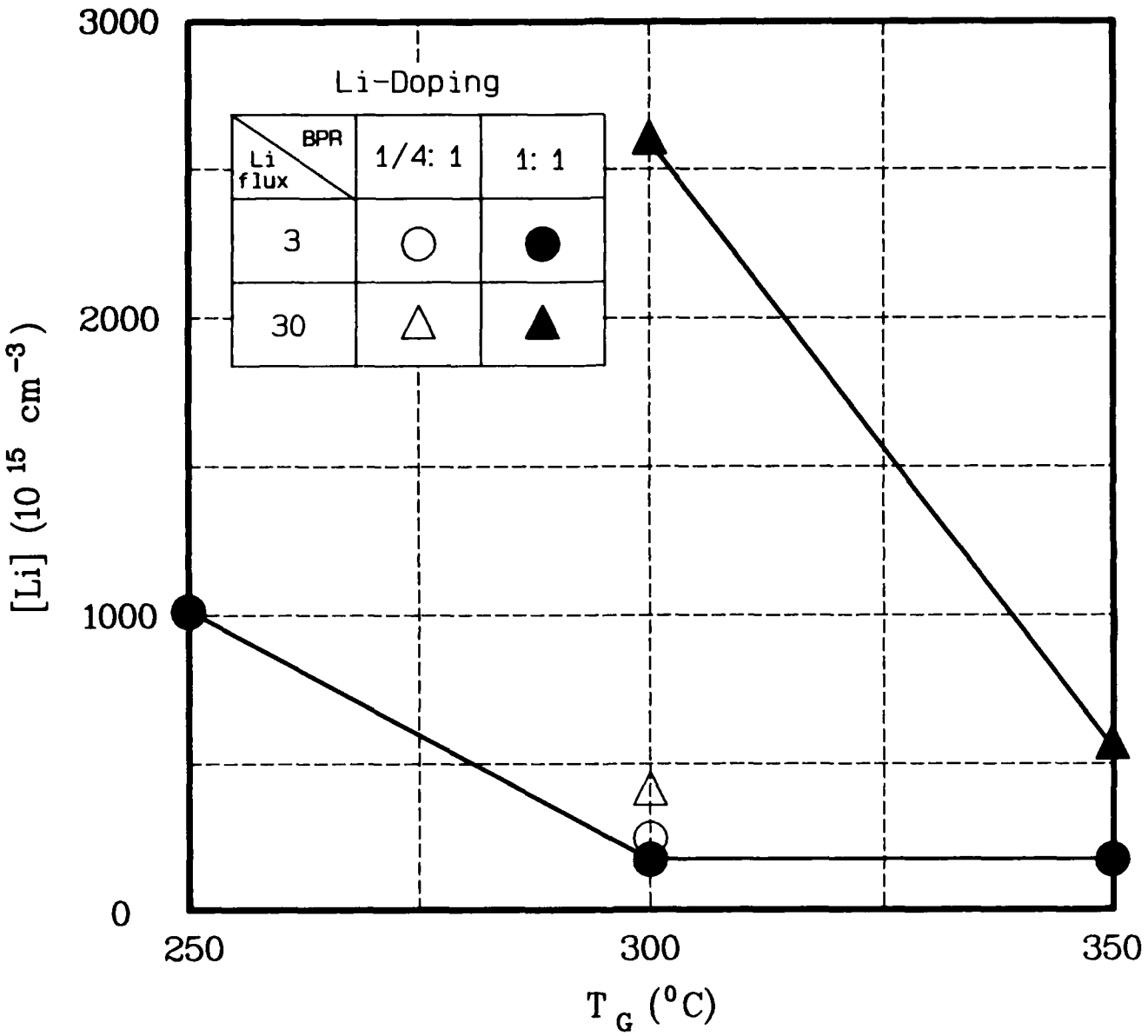

Figure 2-21. Li concentrations, as determined by SIMS, versus substrate temperature during growth. Circles: Li-flux = 3 (arbitrary units). Triangles: Li-flux = 30 (arbitrary units). Solid (open) symbols are for a BPR of 1:1 (1/4:1).

At lower growth temperatures, while there may be higher Li concentrations, these atoms are located on less ideal sites, at which they cannot act as simple acceptors. Unfortunately, measurements of the free carrier concentrations which might support this argument cannot be performed on these high-resistivity samples.

We are quite optimistic about the prospects for Li-doping. We are confident that, once we have accumulated more data from measurements on samples doped from alternate Li sources, we will begin to be able to answer some of the questions raised above.

2.2.3.4 Li-Doping: Electrical Characterization

During this quarter electrical measurements were made on one undoped and eight lithium-doped samples to study the effects of Li incorporation in our MBE-grown ZnSe films. Even though the resistivities of these films were too great to allow routine Hall measurements, information on the electrical properties of the samples was obtained through I-V measurements. The undoped sample was found to be n-type, as expected, and six of the Li-doped films were determined to be p-type; the results were inconclusive for the remaining two Li-doped samples. The I-V measurements also suggested the hole concentrations in these films at room temperature to be near 10^{13} cm^{-3}.

In order to study the electrical properties of our Li-doped ZnSe films both gold and indium were used as contact metals. The Au contacts were deposited in an evaporator with a background pressure of 5×10^{-7} Torr. The thickness of the Au contacts ranged from 1000-2500Å. The In contacts were made by pressing high purity In chips onto the surface of the samples, and then subjecting these samples to various annealing procedures. The sample and contact geometry used in this study is shown in Figure 2-22.

Two-point current versus voltage measurements were made using various combinations of contacts: In-In, Au-Au, In-Au, In-substrate, and Au-substrate. The majority carrier type in each film could then be determined from these measurements since In is known to form Ohmic contact to n-ZnSe [13] and Au forms Ohmic contact to p-ZnSe [14].

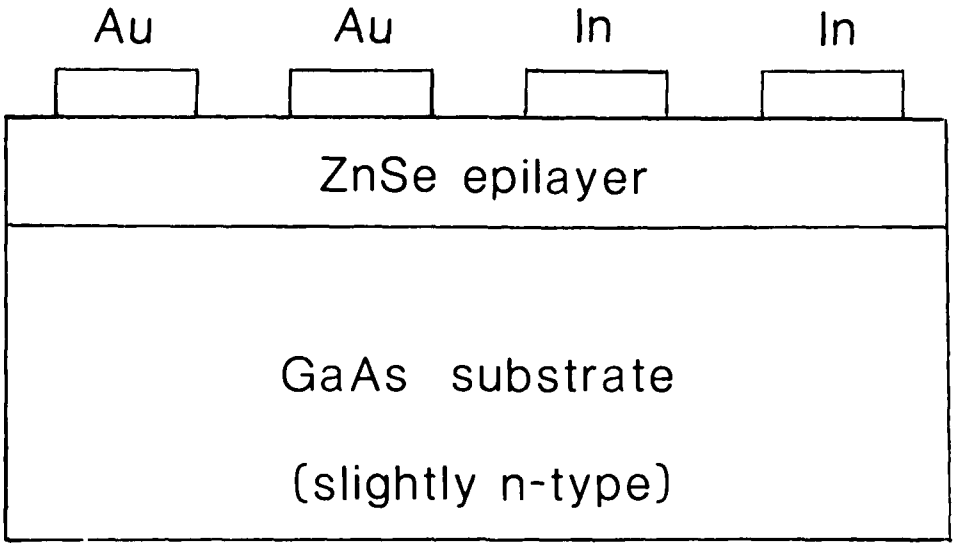

Figure 2-22. Schematic diagram of the sample and contact geometry used in this study.

The I-V measurements obtained for ZSE99A are shown in Figures 2-23 and 2-24. Notice that the I-V for the In-In configuration is linear and the magnitude of current at any voltage is much larger than for the Au-Au configuration. The I-V for the In-Au configuration shows rectifying behavior indicating that one of the metals has formed a Schottky barrier. These three I-V curves require the In contact to be Ohmic and the Au contact to be non-Ohmic; this result implies that ZSE99A is n-type. The result that ZSE99A is n-type is confirmed by the I-V measurement obtained for the In-substrate configuration where the semi-insulating substrate is slightly n-type (Figure 2-25).

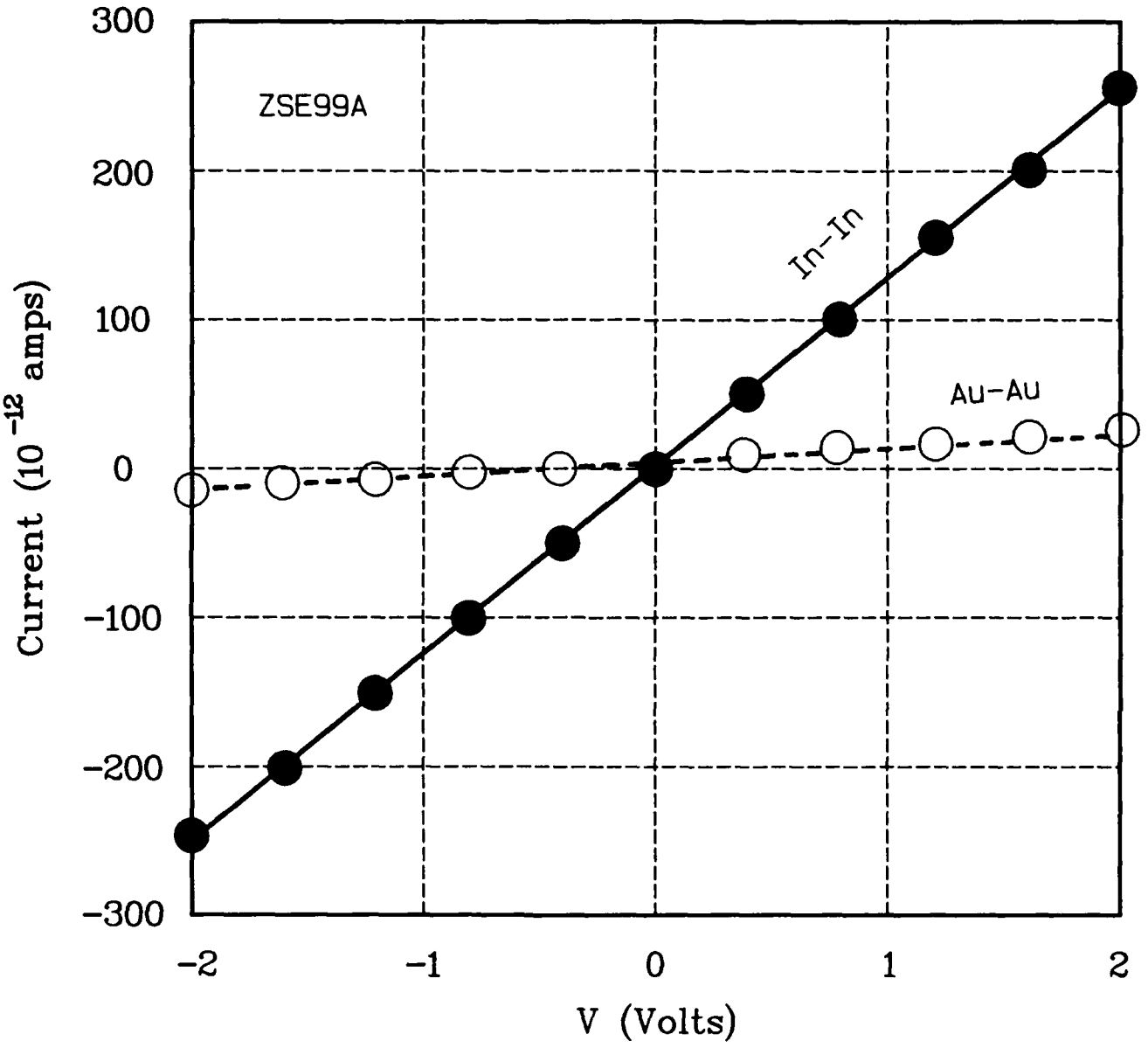

Figure 2-23. I-V characteristic for sample ZSE99A obtained using Au-Au and In-In contacts.

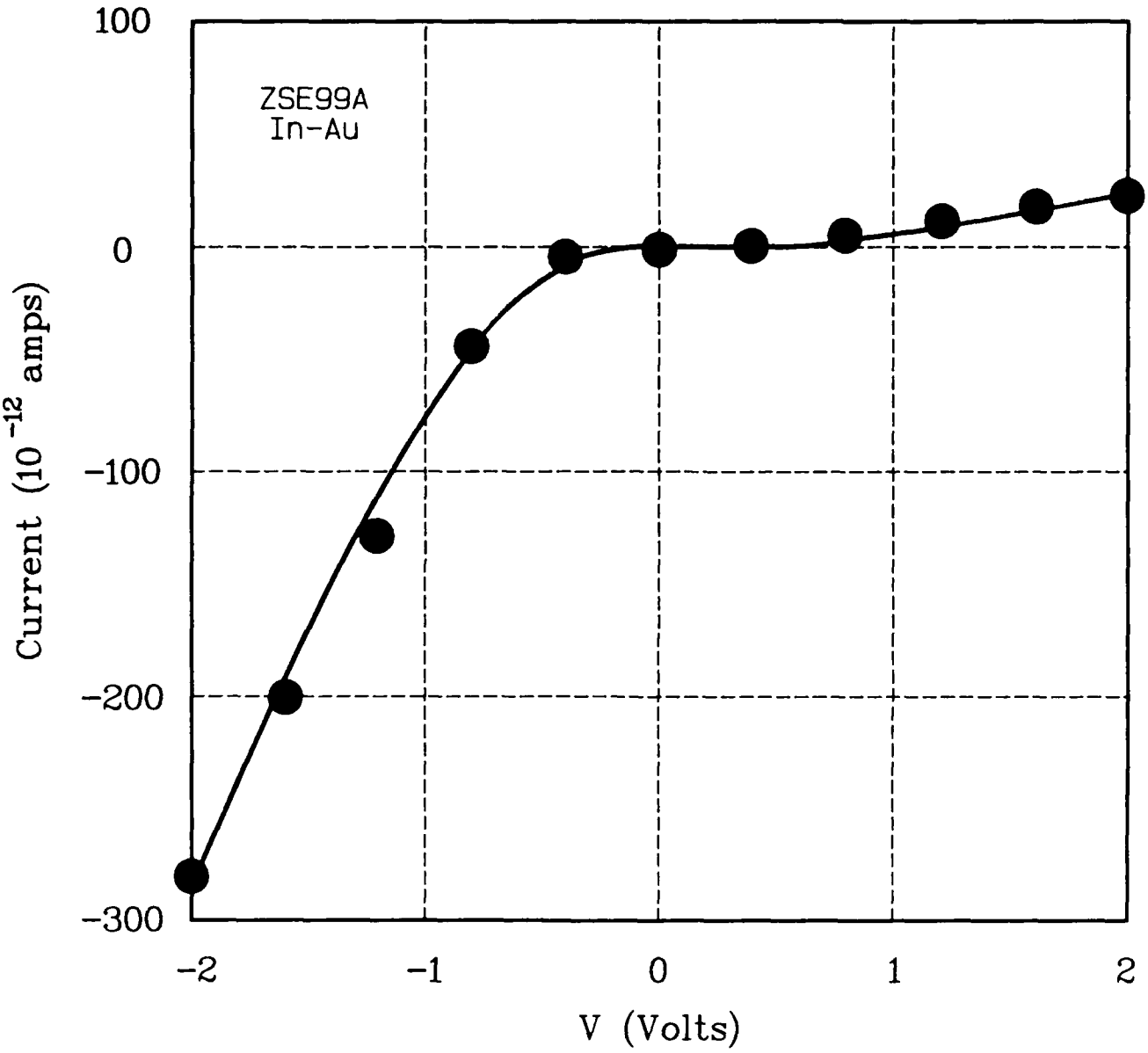

Figure 2-24. I-V characteristic for sample ZSE99A obtained using In-Au contacts. The ordinate is the potential of the In relative to the gold.

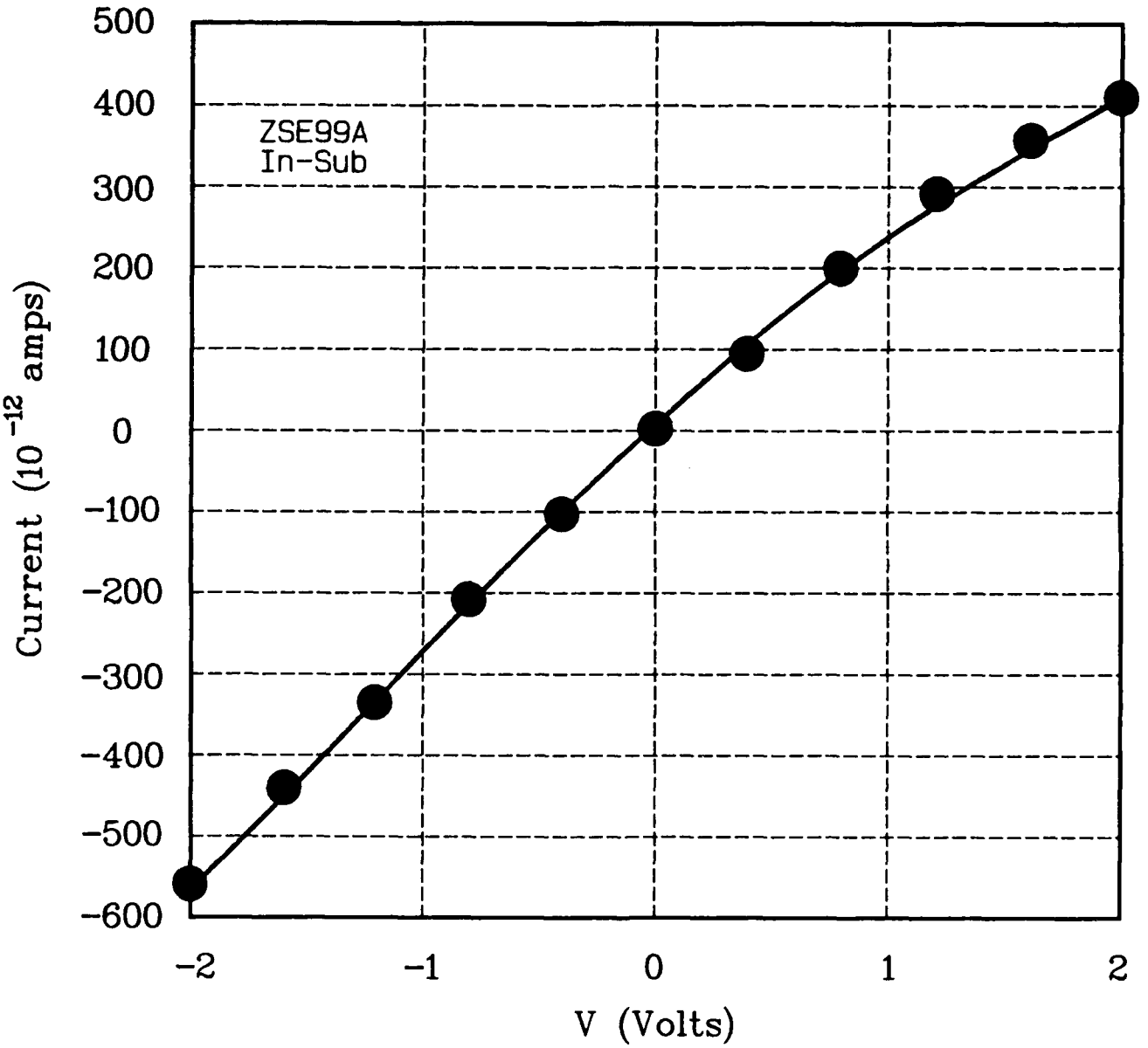

Figure 2-25. I-V characteristic for sample ZSE99A obtained using the In-substrate configuration, where the semi-insulating GaAs substrate is slightly n-type. The ordinate is the potential of the In relative to the substrate. This measurement confirms that the sample is n-type.

The I-V measurements for ZSE101A are shown in Figures 2-26, 2-27 and 2-28. As was the case for ZSE99A the In-Au configuration show that either In or Au forms a Schottky barrier. The I-V's for the In-In and Au-Au configurations suggest that the Au contacts are Ohmic. This implies that ZSE101A is p-type! The I-V measurement using the Au-substrate configuration is consistent with the hypothesis that the ZnSe epilayer is p-type. As is seen in Figure 2-28, the Au-substrate I-V curve shows rectification with the largest current flow occurring when the ZnSe epilayer is positively biased.

Six of the Li-doped samples showed p-type electrical behavior: ZSE100A, ZSE101A, ZSE102A, ZSE103A, ZSE106A, and ZSE107A; the results were inconclusive for ZSE104A and ZSE105A. Although this technique is not quantitative, a lower limit for the hole concentration can be set using the I-V results. If the contact resistance is assumed to be negligible then a resistivity of approximately 90 kΩ-cm is obtained for ZSE101A. A reasonable value for hole mobility (30 - 40 cm^2/volt-sec) gives a hole concentration of 2×10^{12} cm^{-3} for this sample. The largest hole concentration obtained in this manner for the Li-doped samples was 1.2×10^{13} cm^{-3}. Reduced hole mobility values high contact resistance would increase our estimate of p.

2.2.3.5 Li-Doping Summary

In summary, by doping with Li, it has been possible to obtain p-type ZnSe. This is the first report anywhere of p-ZnSe growth by MBE. However, the material being grown is at present high resistivity, with hole concentrations of about 10^{14} cm^{-3}. This is probably due, at least in part, to contaminants being introduced from the Li source. Additionally, it is likely that there is a significant amount of contamination with donors coming from the Se source, as indicated by increased electron concentrations in recent undoped samples.

2.3 Project 2, Task 1: Device Research—Photopumping, e-Beam Pumping, and Cavity Formation

2.3.1 e-Beam Pumping Measurements

In past reports, we have reported the achievement of lasing in ZnSe films grown by MBE on GaAs substrates. At low temperature (15K), transverse

lasing thresholds (J_{th}) as low as 3.9A/cm^2 were observed at an accelerating voltage (V_{acc}) of 20 kV for films only 2 μm thick. More recently, we have prepared thicker films (2 - 5 μm), permitting us to work at higher V_{acc}, and thereby reducing the low temperature threshold to 2 A/cm2. With these reduced thresholds, we were able to observe lasing at temperatures as high as 300K. Here we present a comparative study of the electron-beam-pumped lasing thresholds for films grown by MBE and organometallic VPE (OMVPE). We find that, while the OMVPE films exhibit thresholds that are at least a factor of two higher than those of the MBE films at 35 kV, the difference appears to diminish as V_{acc} increases.

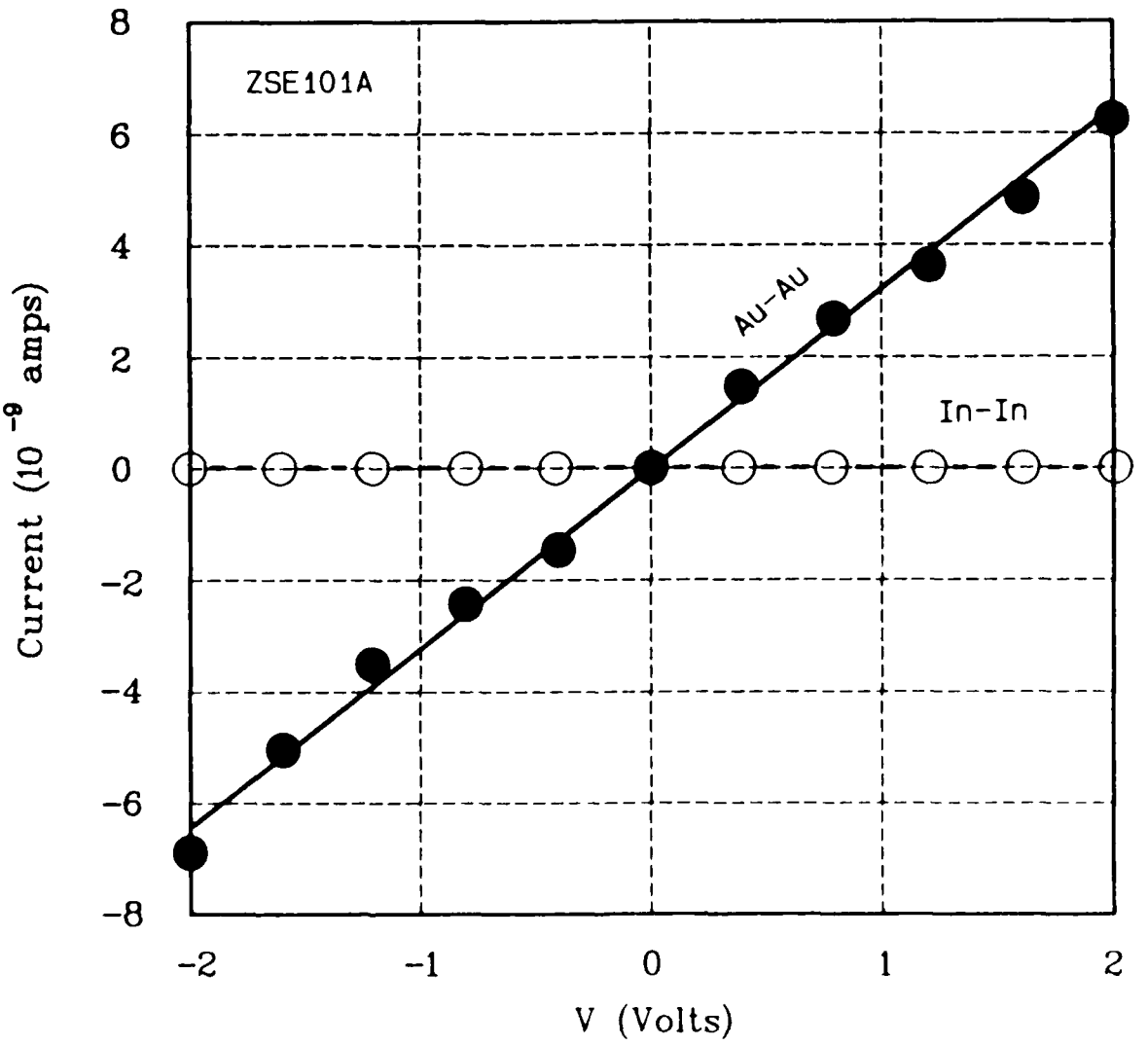

Figure 2-26. I-V characteristic for sample ZSE101A obtained using Au-Au and In-In contacts.

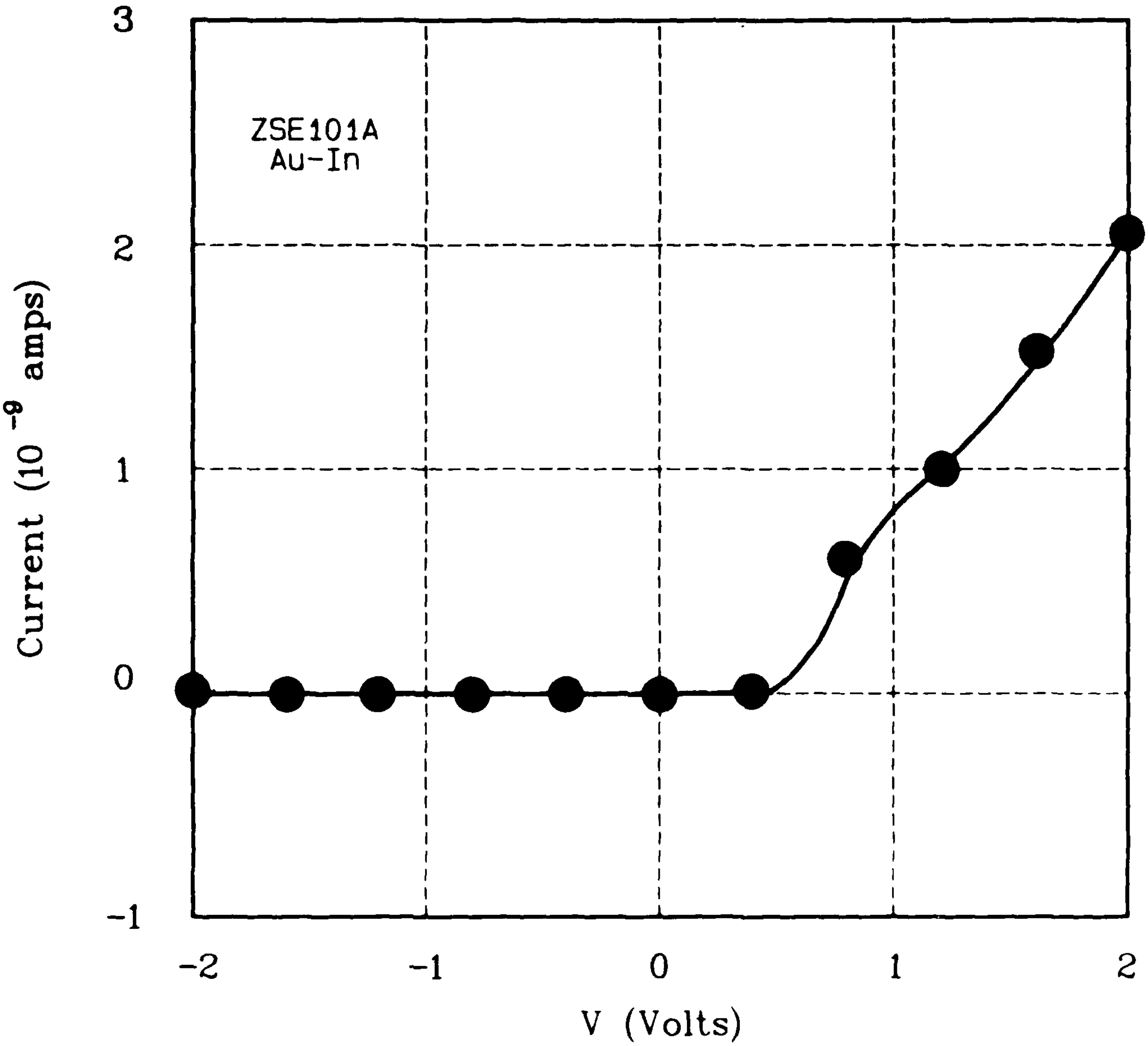

Figure 2-27. I-V characteristic for sample ZSE101A obtained using In-Au contacts. The ordinate is the potential of the Au relative to the In.

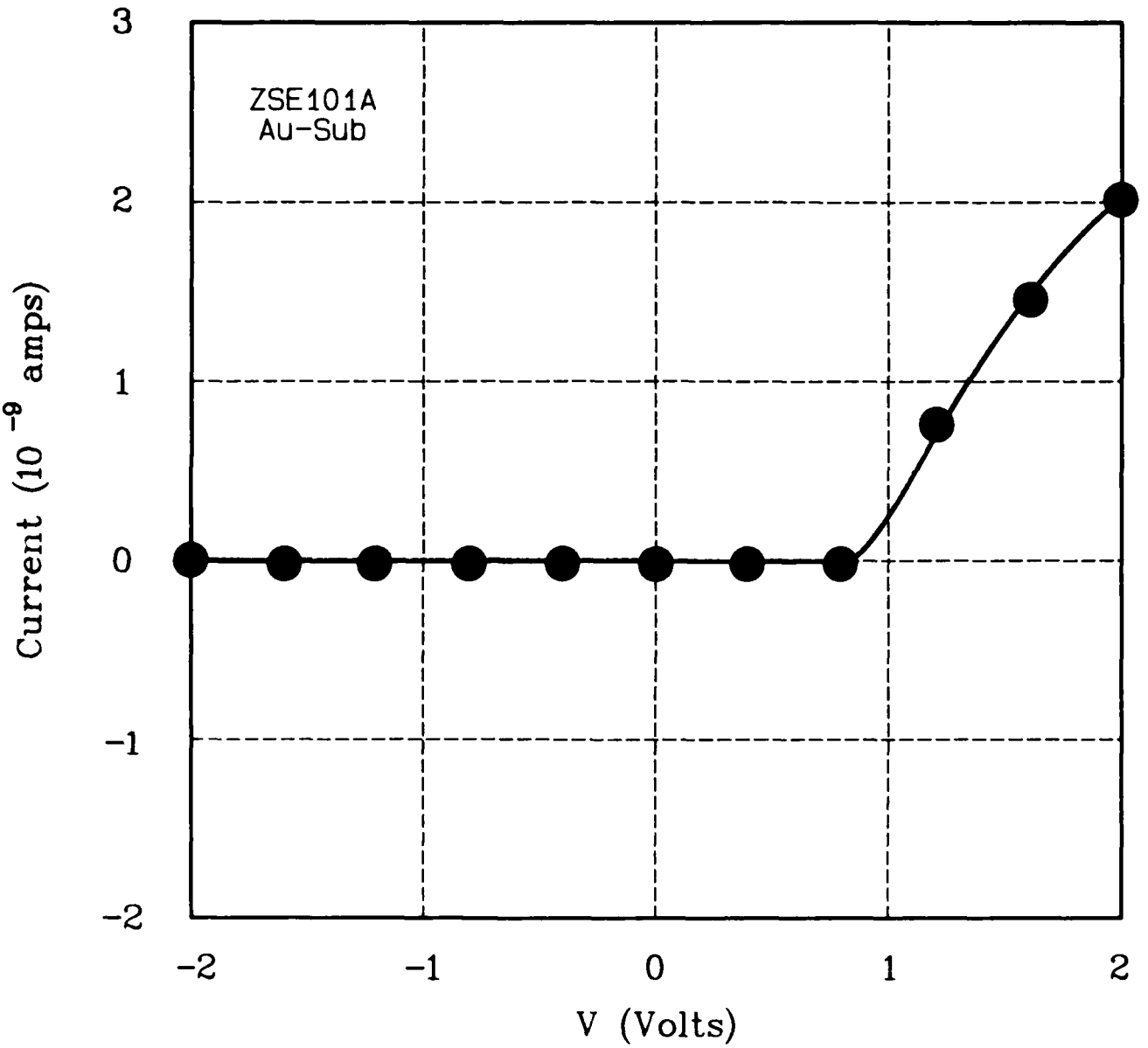

Figure 2-28. I-V characteristic for sample ZSE101A obtained using the Au-substrate configuration, where the semi-insulating GaAs substrate is slightly n-type. The ordinate is the potential of the Au relative to the substrate. This measurement confirms that the sample is p-type!

We argue below that this behavior reflects the poorer surface morphology of the OMVPE films.

Samples for this study were grown by MBE at 3M St. Paul and by OMVPE by Professor B. Wessels at Northwestern University on (100) GaAs substrates. Relevant growth parameters for all the samples are included in Table 2-3. Cavities, formed by mechanically thinning the GaAs to 50 μm and then cleaving along the (110) planes, were 150 - 400 μm long and were held on the Cu cold finger of a closed-cycle helium refrigerator with an In-Ga eutectic. The electron-beam excitation and light detection schemes have been described in previous reports. Resistivity and Hall effect measurements were used to obtain carrier concentrations and mobilities for the MBE films grown on semi-insulating GaAs substrates; for the OMVPE films grown on n^+-GaAs substrates we deduced the carrier concentrations from C-V measurements using Au for a Schottky barrier contact to the ZnSe.

TABLE 2-3.

Growth conditions (substrate temperature (T_g) and Zn-to-Se beam pressure ratio, thickness (t), photoluminescence results (near-band-edge (excitonic) emission intensity (NBE), deep level emission intensity (DL), and the ratio of NBE-to-DL intensities (R), 300K electron carrier concentrations (n), and measured threshold electron-beam-current densities (J) for MBE and OMVPE films. NL means that no lasing could be obtained in cavities made from these films.

Sample	Growth Method	T_g (°C)	Zn/Se	t (μm)	NBE intens (c/s)	DL intens (c/s)	R	n (cm^{-3})	J (A/cm^2)
Y140	OMVPE	280	0.5	6.0	3400	44	78	$4.2X10^{16}$	15
Y141	OMVPE	289	0.5	6.2	28000	530	52	$4.2X10^{16}$	5-13
Y142	OMVPE	280	0.5	4.6	10000	120	83	$2.1X10^{1}$	NL
Y143	OMVPE	280	0.5	4.5	3700	170	22	$1.6X10^{16}$	4-15
Y144	OMVPE	280	0.4	3.1	26000	30	830	$5.0X10^{1}$	NL
Y145	OMVPE	280	0.33	3.4	6600	53	125	$1.2X10^{16}$	NL
ZSE48A	MBE	350	0.5	4.35	18000	25	700	$3.3X10^{1}$	1-3
ZSE88A	MBE	350	0.5	4.2	1950	60	33	$< 1X10^{14}$	2-3

In our earlier studies, we demonstrated lasing in MBE-grown films with thicknesses between 2 and 5 μm; for the present study, we concentrated on just those MBE films with thickness greater than 4 μm, in order to compare with the OMVPE films. Lasing was achieved in the two MBE-grown films and in three of the six OMVPE films studied here. The evolution of the cathodoluminescence (CL) spectra with increasing current density from a broadened spontaneous emission to a narrow peak at the onset of lasing is demonstrated for an MBE and an OMVPE film in Figure 2-29 (a) and (b), respectively. Figure 2-30 shows the measured linewidths for these same two samples. Note the much greater width of the lasing peak in the case of the OMVPE sample. Typical measurements of the integrated light output versus incident current density are plotted in Figure 2-31. The lasing threshold, indicated by a vertical arrow in Figure 2-30 or 2-31, was taken to be that current density at which the (low-current) linear and (high-current) superlinear portions of the curve intersect on a log-log plot. While the MBE films exhibited low-temperature thresholds as low as $1 A/cm^2$ at V_{acc} = 35 kV, thresholds for the OMVPE films were always at least a factor of three larger than this. In attempting to identify the origin of this difference, we have compared the optical, electrical, and surface morphological properties of the two types of films.

Our PL measurements yielded qualitatively similar results for all of the films studied here. These data are summarized in Table 2-3. In all cases, the near-band-edge (NBE) exciton-related emission was dominant, there was no measurable donor-acceptor-pair (DAP) emission, and the deep-level (DL) emission was weaker than the NBE emission by a factor (R, in Table 2-3) which varied between 20 and 800. Various defects introduce deep electronic levels in ZnSe which can trap carriers or lead to deep-level (DL) radiative recombination which might detract from the efficient production of near-band-edge (NBE) emission which is needed for lasing. However, these DL processes are known to be quite slow, with characteristic decay times orders of magnitude larger than excitonic recombination processes, and can readily become saturated. One would not expect, therefore, to see any correlation between the lasing threshold and the intensity of DL emission observed in PL measurements.

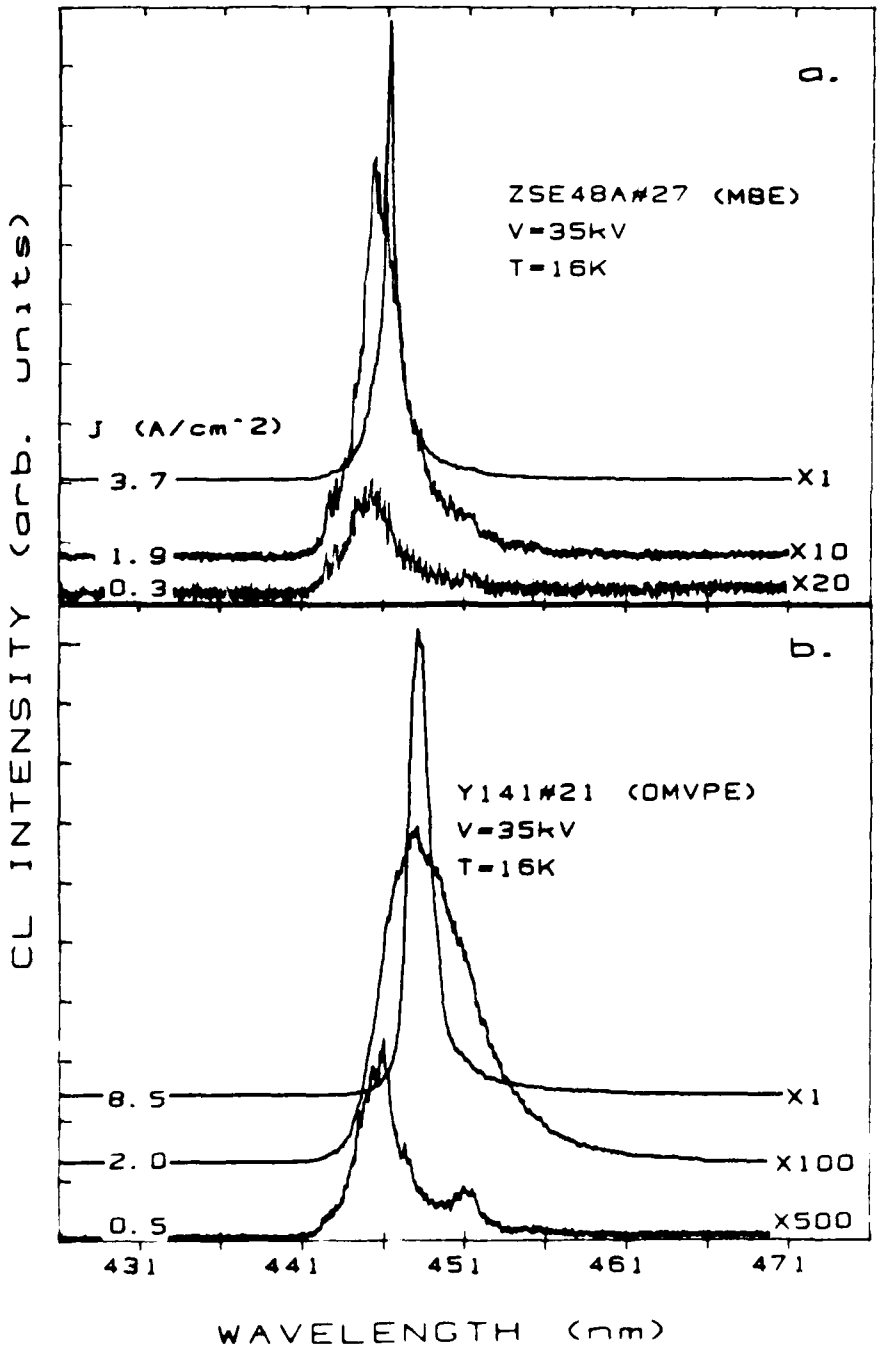

Figure 2-29. Spectral output of ZnSe films prepared by (a) MBE, and (b) OMVPE for differing incident electron beam current densities as indicated. Measurements were made by a gated OMA at T = 16K with an accelerating voltage of 35 kV.

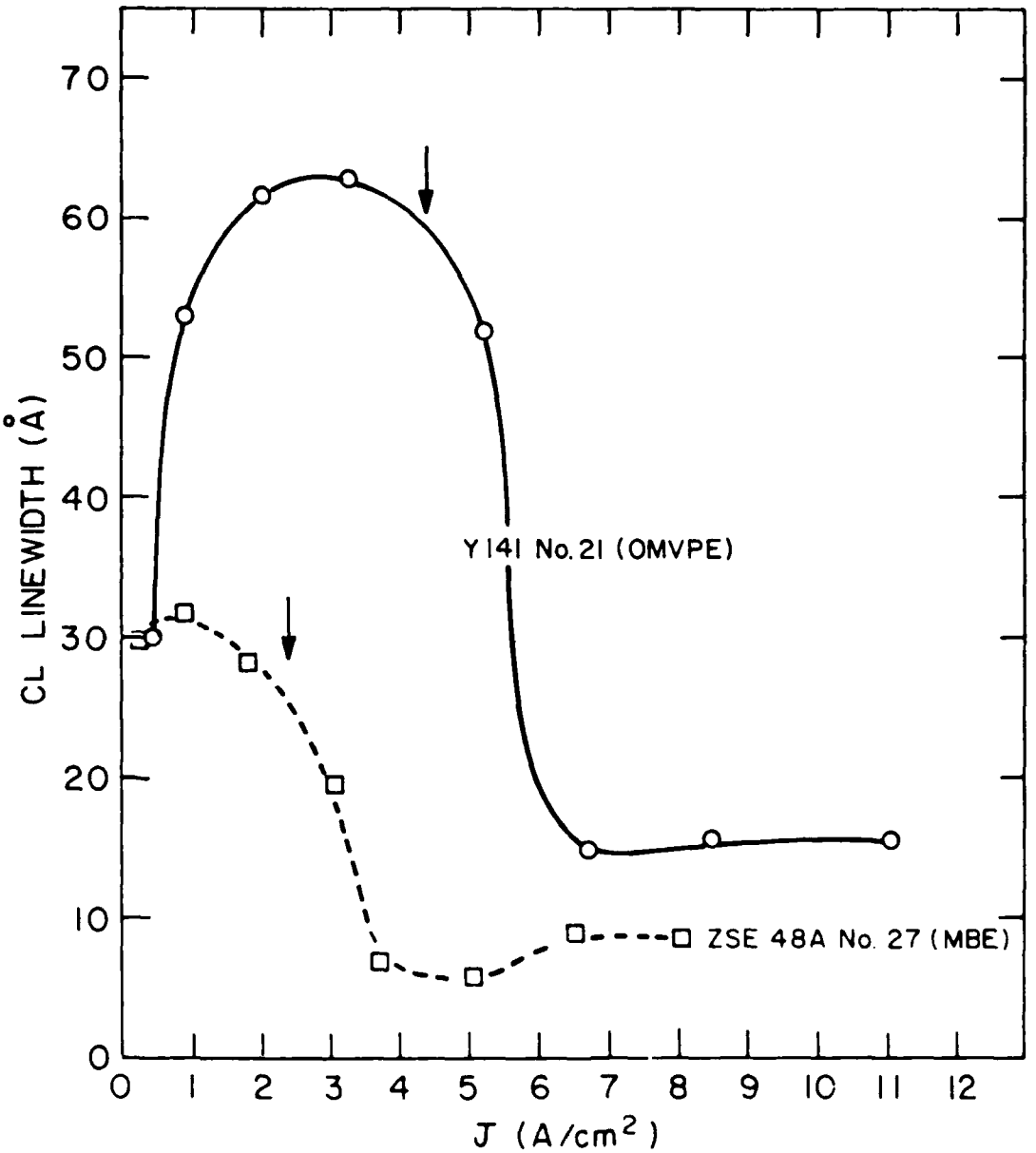

Figure 2-30. Measured cathodoluminescence linewidths (FWHM) versus electron beam current densities for electron-beam-pumped cavities formed from an MBE (squares) and an OMVPE (circles) film. Lasing thresholds are indicated by vertical arrows.

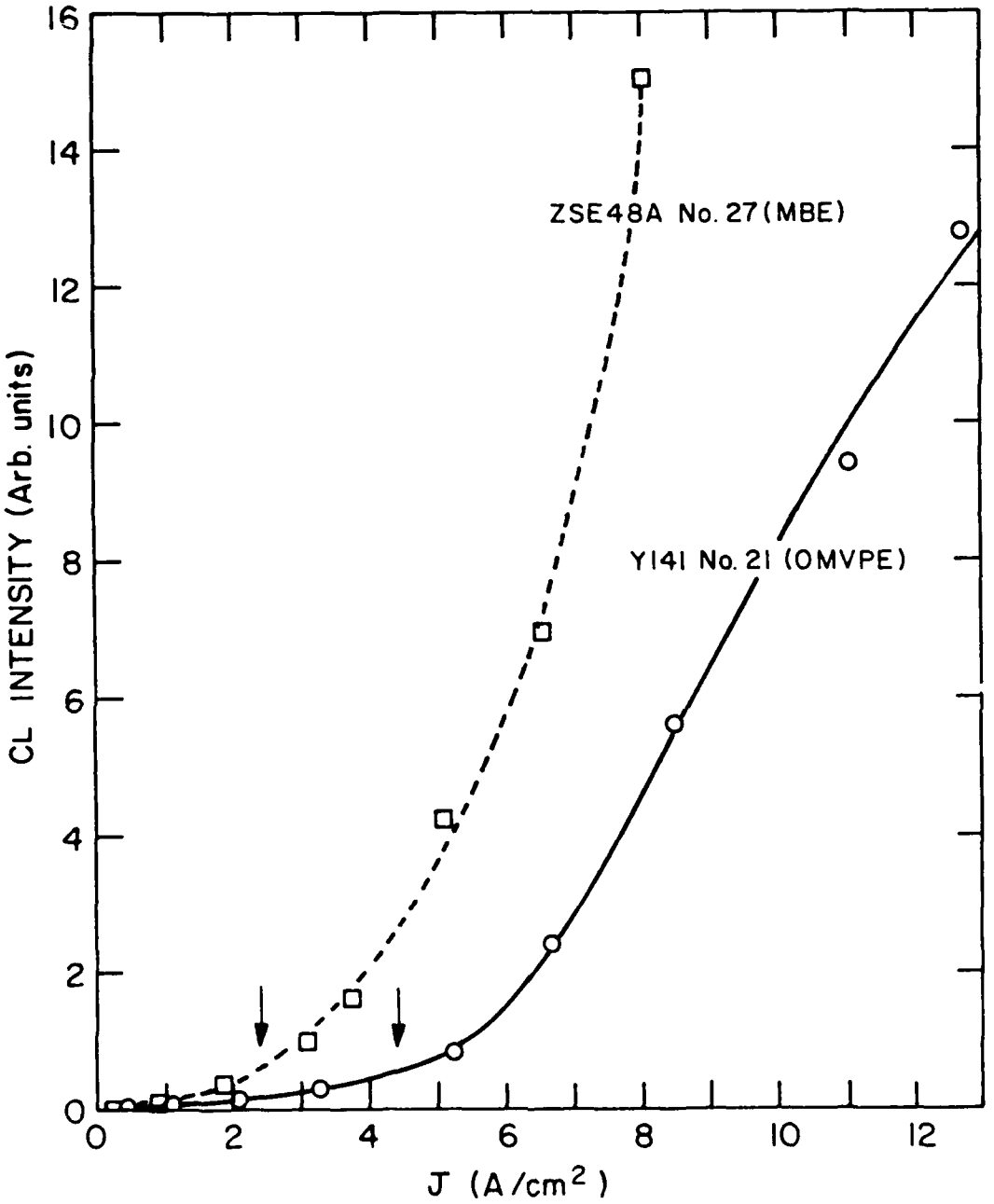

Figure 2-31. Integrated light output versus incident electron beam current density for electron-beam-pumped cavities formed from an MBE (squares) and an OMVPE (circles) film. Lasing thresholds are indicated by vertical arrows.

It is less clear, however, whether there might not be a correlation between a low lasing threshold and a large NBE emission intensity. As the data in Table 2-3 indicate, we have observed lasing in samples which varied widely in the magnitude of their NBE PL emission intensity. We find no correlation between the lasing threshold and the NBE PL intensity. This is best demonstrated by comparing the data for the two MBE samples (ZSE48A and ZSE88A) of nearly equal thicknesses; the lasing thresholds are identical in spite of the large difference (X50) in their NBE emission intensities.

Since we were unable to measure majority carrier mobilities in the OMVPE films grown on n^+-GaAs substrates, we have only our measurements of carrier concentrations to compare (see Table 2-3). Again, we see no correlation with the lasing threshold; samples differing in carrier concentration by more than a factor of 300 exhibit the same lasing thresholds.

We did find significant differences, however, in the surface morphologies of the films. Typical SEM photographs of the films (Figure 2-32) show that most of the OMVPE films have a wavy, textured surface with elongated features of approximate dimensions 0.5 μm x 5 μm; these films appear hazy to the naked eye. For films #Y144 and Y145 this surface texture is diminished and the films appear less hazy. Unfortunately, their smaller thicknesses increase the electron-beam-pumped lasing thresholds for the reasons we have discussed in earlier reports, making a comparison with the thicker films difficult. In contrast to the OMVPE films, the MBE films display no discernible structure at this magnification.

We feel that it is the variations in the surface morphologies of the films discussed above which accounts for the observed differences in the electron-beam-pumped lasing thresholds. In electron-beam excitation, particularly at low electron accelerating voltages where a large fraction of the excitation energy is deposited near the surface, the optical quality of the surface must be sufficiently high to support the reflection of laser modes within the cavity (the quality of this surface is even more important in the case of an optically-pumped cavity).

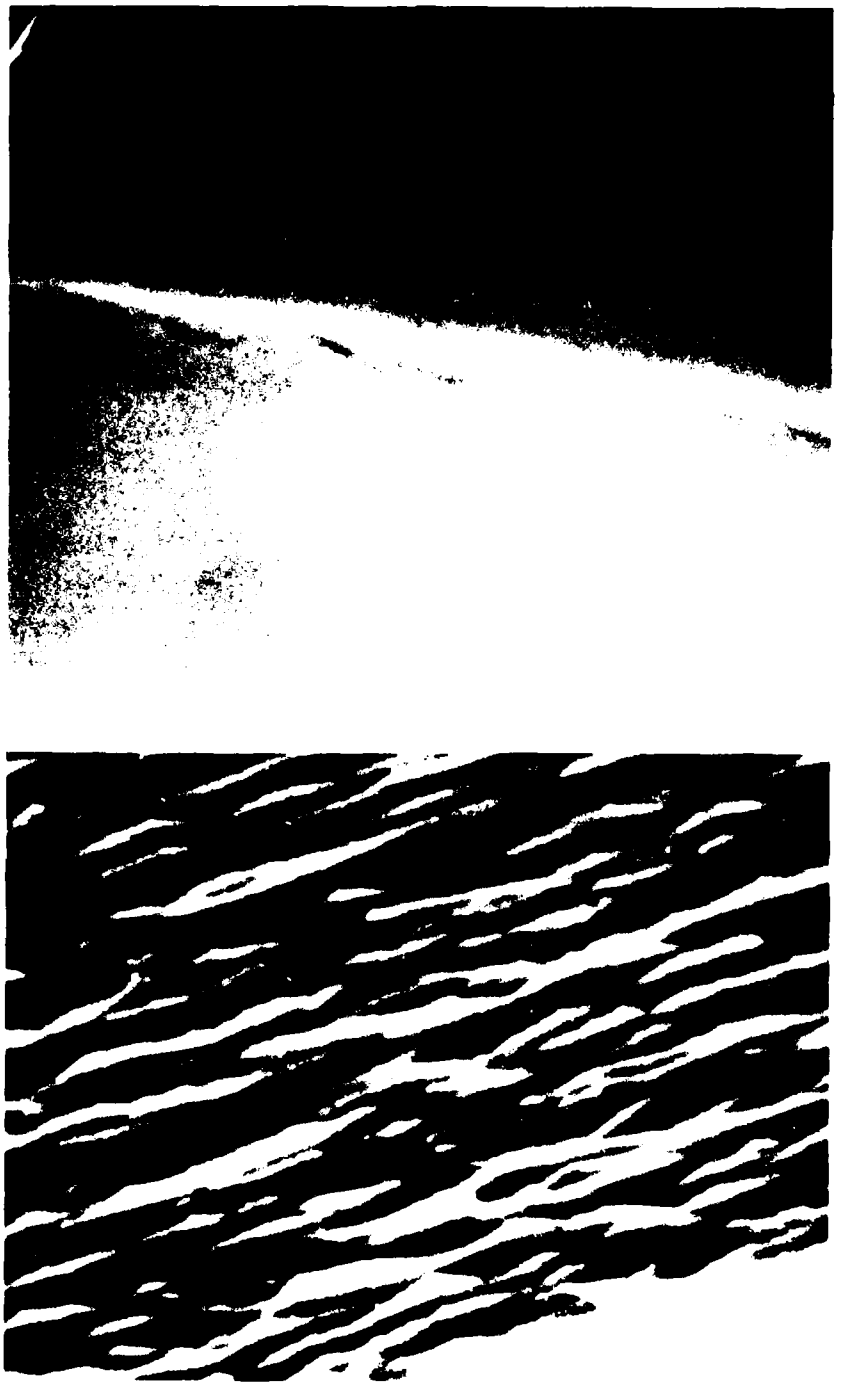

Figure 2-32. SEM photographs of the surfaces of an (a) MBE and (b) OMVPE film near a cleavage plane. Along the cleavage surface, the ZnSe film can be distinguished from the GaAs substrate. Elongated features with typical dimensions 0.5 μm x 5 μm produce a wavy texture on the surface of the OMVPE films. The magnification is approximately 4000X for both photographs.

The gross features on the surface of the OMVPE films serve to scatter rather than internally reflect the cavity modes, thereby introducing additional losses which drive the required threshold current upward. Figure 2-33 shows the how the threshold current density varies with V_{acc} for an MBE and an OMVPE sample. For the MBE film, the threshold increases monotonically with decreasing V_{acc}. The dashed line shows the V_{acc}^{-1} dependence expected if the required threshold power were constant; i.e., if the cavity losses were independent of the incident electron energy. Clearly, the measurements indicate that the threshold power increases more rapidly than this. At low V_{acc}, the reduced penetration depth of the incident electrons will lead to increased losses due to diffraction, surface recombination, and surface scattering. These increased losses are reflected in the rise of the measured thresholds above those predicted on the basis of a constant threshold power. For the OMVPE film shown in Figure 2-33, the increase of the lasing threshold with decreasing V_{acc} is much more rapid than for the MBE film, becoming unmeasurably high for V_{acc} = 30 kV and below. The PL results indicate that the texture on the OMVPE film surfaces does not significantly increase the surface recombination rate, since MBE and OMVPE films of comparable quality (as judged by PL linewidths and R-values and residual carrier concentrations) exhibit comparable radiative efficiencies. Rather, we believe the data of Figure 2-33 to lend further support to our postulation of greatly increased surface scattering losses in the OMVPE film cavity because of the poorer surface morphology.

Given the magnitude of the losses introduced by the surface texture of the OMVPE films, it is likely that we were observing a superradiant, rather than a lasing, behavior for most of these samples. This is suggested by the less abrupt turn-on of the light output at threshold (Figure 2-29), as well as by the consistently larger spectral peak widths observed above threshold for the OMVPE films as compared to the MBE samples(Figure 2-30), similar to the behaviors displayed by superluminescent diodes [15].

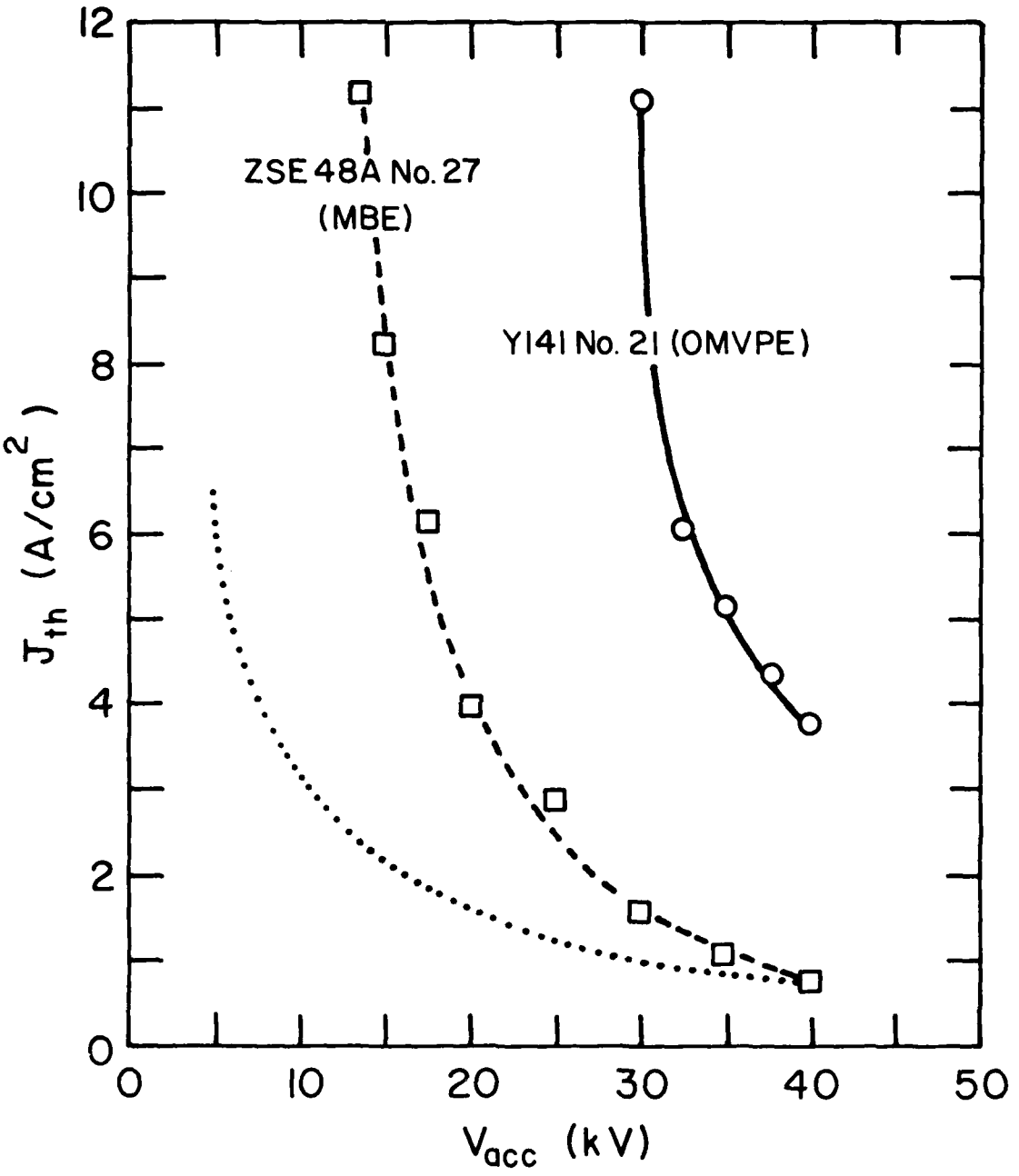

Figure 2-33. Threshold current densities versus electron accelerating voltage for an MBE (squares) and an OMVPE (circles) film. The dotted line represents a $1/V_{acc}$-dependence which would result if the required threshold power were constant at the 40 kV value (approximately 35 kW/cm^2). The increased losses encountered at smaller V_{acc} are discussed in the text.

In summary, it would appear that both of these low-temperature deposition processes produce ZnSe epitaxial films sufficiently free of strains and defects (as evidenced by high PL efficiency and narrow excitonic linewidths and high electrical mobility) to significantly reduce the lasing thresholds below those reported for material grown by higher-temperature techniques.

2.4 Project 2, Task 2: Contact Studies

2.4.1 Maximization of Performance of ZnSe-ZnS_xTe_{1-x} (x = 0.37) Heterostructures

It has been shown [16] that the ZnSe-ZnS_xTe_{1-x} (x = 0.37) heterojunction has the ability to confine a 2DEG in the ZnSe at this lattice-matched heterointerface. Owing to the large conduction and valence band offsets, confinement is very efficient and leads to promising transport characteristics for this junction, with future applications potential for blue-light-emitting devices.

In this work, a theoretical model for electron transport in the 2DEG confined by a triangular potential at the ZnSe heterointerface was formulated. The dependence of the electron mobility on the undoped spacer width was calculated, including all major scattering mechanisms: these include phonons (acoustic, piezoelectric and optical), impurities (background and remote ionized impurities) and alloy disorder scatterings. Intersubband scattering was also found to play an important role [16], especially at higher areal densities and was included. In a previous report [16], the dependence of the electron mobility on areal density and doping was discussed. Thus considering the influence of spacer width on scattering, all possible physical or structural parameters which affect transport in this structure are considered.

The basic consideration of the modulation doped heterostructure is to separate the 2DEG from parent ionized donors thereby limiting remote ionized impurity scattering; that is the spacer width, d, should be maximized. However, since as the d value increased the efficiency of electron transfer to the 2DEG decreases, the areal density in the well will decrease and have

a deleterious effect on the electron mobility [16]. Clearly then, the electron mobility should have a complex behavior determined by an interplay between these two factors. In fact, the key consideration in device applications of these structures is to maximize the channel conductivity, $N_s e\mu_e$.

Figure 2-34 gives the maximum inherent channel conductivity σ_{max}^{inh} as a function of spacer width: σ_{max}^{inh} has been maximized with respect to N_s at a given d value. In this figure, N_s and N_i^b values required to maximize σ are also given. The rapid rise in σ at small d to about 20 $(m\Omega)^{-1}$ at around 50Å reflects the competing influence of electron transfer and ionized impurity scattering discussed earlier. Indeed higher N_i^b shifts the mobility to successively lower d values, thereby resulting in lower σ values. The ionized impurity scattering is especially sensitive to the ionized impurity distribution function: if diffusion of the doping profile exists, this would have a very profound effect at smaller d values. Insight has thus been gained into the very practical decisions that must be made on choice of d values.

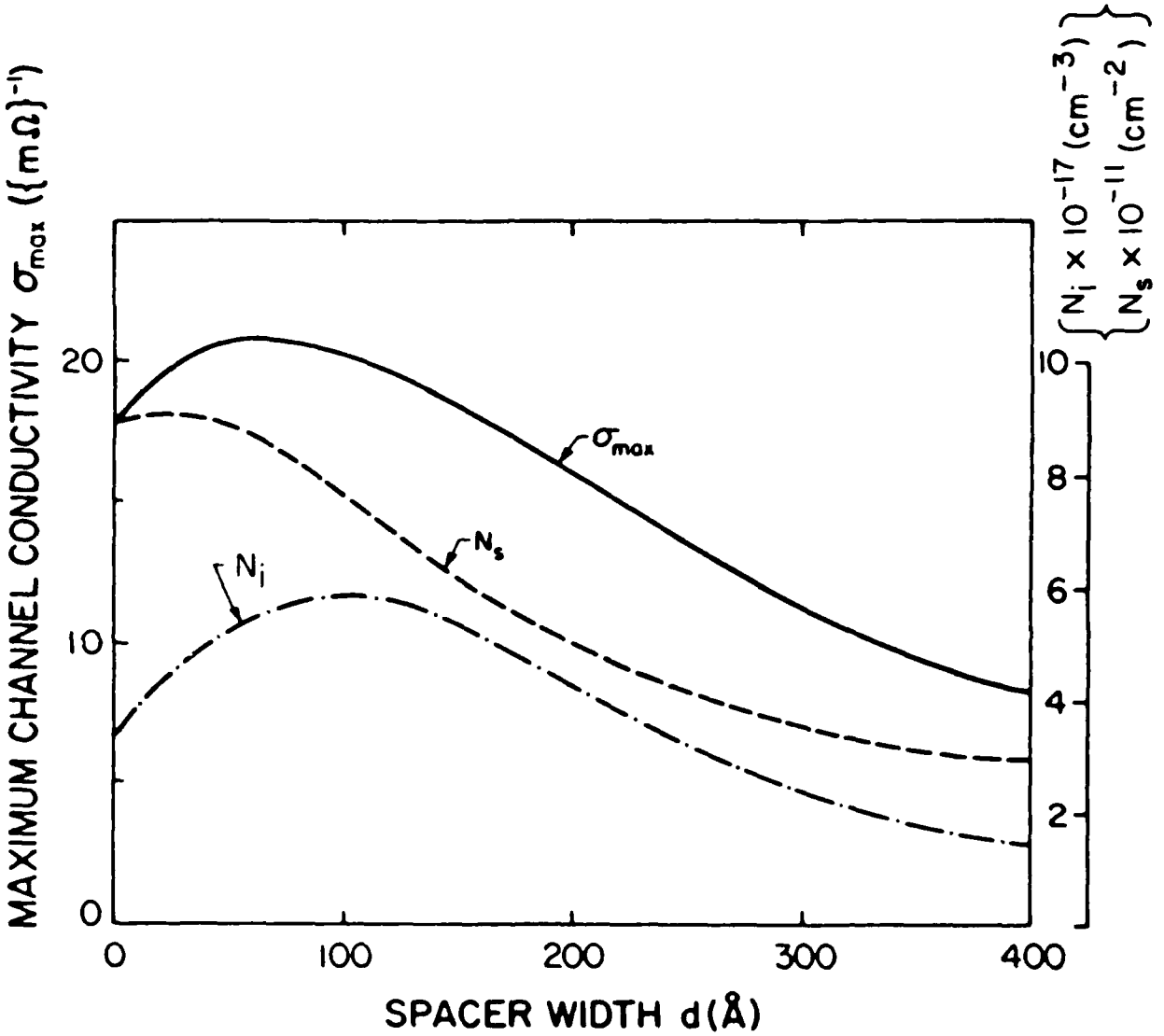

Figure 2-34. Maximum inherent channel conductivity versus spacer width.

3.0 REFERENCES

1. H. Nagai, J. Appl. Phys. 45, 3789, (1974).

2. J. Kleiman, R. M. Park, H. A. Mar, to be submitted to Appl. Phys. Lett.

3. J. W. M. DuMond, Phys. Rev., 52, 872, (1937).

4. T. Hattanda and A. Takeda, Japan. J. Appl. Phys., 12, 1104, (1973).

5. O. Nittono and S. Shimizu, J. Cryst. Growth, 45, 476, (1978).

6. T. Vreeland, Jr., J Mat. res., 1, 712, (1986).

7. S. B. Sant, J. Kleiman, M. Melech, R. M. Park, G. C. Weatherly, R. W. Smith and K. Rajan, in proceedings of 5th Oxford Conference on Microsco py of Semiconducting Materials, Oxford, 6-8 April, 1987, in the press.

8. S. Myhajlenko, J. L. Batstone, H. J. Hutchinson and J. W. Steeds, J. Phys. C : Solid State Phys 17, 6477 (1984).

9. J. Nishizuwa, K. Itoh, Y. Okuno and F. Sakurai, J. Appl. Phys. 57, 2210 (1985).

10. T. Yasuda, I. Mitsuishi and H. Kukimoto, 34th Spring Meeting Jpn. Soc. Appl. Phys. and Related Societies; Tokyo; 1987.

11. Quarterly Technical Progress Report No. 3.

12. T. Mitsuyu, K. Ohkama and O. Yamazaki. Appl. Phys. Lett. 49, 1348 (1986).

13. G. Jones and J. Woods, J. Phys. D: Appl. Phys. 9, 799 (1976).

14. G. Stringfellow and R. Bube, Phys. Rev. 171, 903 (1968).

15. T. P. Lee, C. A. Burrus, Jr., and B. I. Miller, IEEE J. Quant. Electr., Qe-9, 820 (1973).

16. H. Ruda, J.A.P. 49, 35 (1986).

END

9-87

DTIC